DOI 10.1007/s11106-021-00254-w
Powder Metallurgy and Metal Ceramics, Vol. 60, Nos. 7-8, November, 2021 (Russian Original Vol. 60, Nos. 7-8, July-August, 2021)

THEORY AND TECHNOLOGY OF SINTERING, THERMAL AND THERMOCHEMICAL TREATMEN

THE DEVELOPMENT AND APPLICATION OF SPARK PLASMA SINTERING TECHNIQUE IN ADVANCED METAL STRUCTURE MATERIALS: A REVIEW

X.Y. Li,[1,2] Z.H. Zhang,[1,3,4] X.W. Cheng,[1,3] G.J. Huo,[1] S.Z. Zhang,[1] and Q. Song[1]

UDC 621.762.5

Spark plasma sintering (SPS) is a type of pulsed electric current-assisted sintering technique. This method allows for rapid consolidation of powder materials into dense bulk when simultaneously applying uniaxial pressure and pulsed electrical current in a vacuum or protective atmosphere. Many scholars and researchers have realized the importance of the SPS due to its significant advantages in controlling the powder surface condition, atomic diffusion, phase stability, and crystal growth behavior. All these features inevitably influence the densification behavior and resulting physical and mechanical properties of the sintered materials. This review represents an extensive introduction of recent developments and fundamental principles in SPS techniques after a general description of the method and its outstanding advantages. A possible design for the SPS technique is proposed as well. Subsequently, the effects of each operating parameter, including current, voltage, and uniaxial pressure, on the densification behavior of advanced metals and alloys under various sintering conditions are reviewed. Finally, the successful applications of the SPS in preparing novel metal structural materials, such as high-quality special steels, new lightweight alloy materials with high performance, high entropy alloys, and other metal alloys, are described in detail.

Keywords: *spark plasma sintering, densification behavior, heating mechanisms, metal structure materials.*

INTRODUCTION

Spark plasma sintering (SPS), also known as field-assisted sintering technique (FAST), plasma-activated sintering (PAS), or pulsed electric current sintering (PECS), is a newly developed type of electric discharge sintering technique belonging to the range of powder metallurgy (PM) methods [1–3]. The resourceful SPS mainly features the combination of plasma generation under simultaneous heating and uniaxial pressure and can be accomplished

[1]School of Materials Science and Engineering, Beijing Institute of Technology, Beijing, 100081, PR China. [2]School of Physics and Electronic Information, Yan'an University, Yan'an 716000, PR China. [3]National Key Laboratory of Science and Technology on Materials under Shock and Impact, Beijing, 100081, PR China.
[4]To whom correspondence should be addressed; e-mail: zhang@bit.edu.cn, lxyissp@126.com.

Published in Poroshkova Metallurgiya, Vol. 60, Nos. 7–8 (540), pp. 32–66, 2021. Original article submitted September 24, 2020.

quickly due to distinctive heating mode [4–7]. That is a distinctive feature of this method compared to traditional PM methods like hot pressing and hot isostatic pressing characterized by long duration and subsequent high-temperature heat treatments. Based on the unique heating mechanism, the benefits of the SPS method in preparing metal structure materials can be briefly summarized as follows.

- *Higher heating rate.* The heating process involved in SPS depends on the initial state and intrinsic powder properties, size and shape of the die, equipment capacity, and heating mode [8]. To our knowledge, most SPS devices are equipped with a DC pulse generator, which can supply pulsed DC to unconsolidated powder compact. During the heating process, the impulse currents pass directly through the compact conducting powder and the die without the entire furnace chamber, which effectively reduces the heating zone. Additionally, electrical discharge can be caused at the contact points of metal powder particles by the direct pulsed current flow, resulting in self-heating of the powders due to the joule effect [9]. Furthermore, plasma could be generated at the gap of powders in this heating process, subsequently producing local high temperatures, which causes surface evaporation and melting of the powders and promotes sintering densification [10]. However, more robust evidence is needed to demonstrate whether plasma is formed between particles. Due to the above reasons, the heating rates of most SPS devices are quite high, achieving up to 1000 °C/min [8]. It is also indicated that the grain growth at the early SPS stages could be effectively inhibited because of the high heating rate [11]. Essentially, it needs adequate time to reach equilibrium for the newly formed grain boundaries, which could not be provided by the rapid heating process [12]. Just because of its conciseness and rapidity, SPS has become quite influential in researching and designing materials.
- *Lower densification temperature.* Some publications have reported that the densification temperature of the SPS process is approximately 200–300°C lower than during traditional sintering. That is mainly attributed to different diffusion mechanisms. In the sintering process, the faster diffusion might be caused by the combination of surface activation of the powders and increased contact between the metal particles. Besides, the increment in SPS local temperature results in high plastic flow rates and decreases the strength of metallic powders, which enhances the creeping flow [13]. Simultaneous pressure application can also facilitate this plastic flow and ensure good contact between metal particles. Based on the above, better necks between metallic particles can be easily formed, reducing densification temperature [14]. As such, the SPS technique is very suitable to fabricate hard-to-sinter materials, such as refractory metals and alloys (W and Mo) [14, 15] with high melting points and ceramic materials [16–18] since all of them require high sintering activation energy.
- *Shorter holding time.* In most conventional sintering methods, a holding time of several hours or longer is commonly needed to obtain bulks with desired density. However, the holding time of only several minutes is enough for the SPS. According to the correlative research, the incremental changes in SPS dwell time effectively decrease the viscosity of metal powders, resulting in simultaneous structural relaxations and significantly enhancing the density of the compact [19]. In the current research group's work, 3 min is required to obtain pure Ti bulk with a homogeneous microstructure and desired density of 99.8%. According to Raichenko et al. [20], only 45 sec is required to obtain Cu–50Ni composite bulks with a homogeneous microstructure, while isothermal sintering needs a holding time of 4 h. The extended holding time can effectively reduce material defects and improve density, increasing physic and mechanical properties. However, some studies have also revealed that the incremental changes in SPS dwell time do not always increase densification. Indeed, a longer SPS dwell time has a reducing effect on the densification of metal materials. It is shown that for the spark plasma sintered nanocrystalline and commercially pure (CP) Ti, higher strength and ductility were obtained for the sample sintered for 3 min of dwell time than that sintered for 5 min [21]. The longer dwell time is thought to cause grain coarsening and eliminate the nonequilibrium microstructure [22] due to the thermal recovery effect, which usually provides better strength and ductility in fine-grained structures [23].

It was also observed that the incremental changes in SPS dwell time slightly degrades the densification of pure copper due to expansion and obturation of the gases absorbed on the surface of Cu powders during the plastic deformation in the early sintering stages [24, 25].

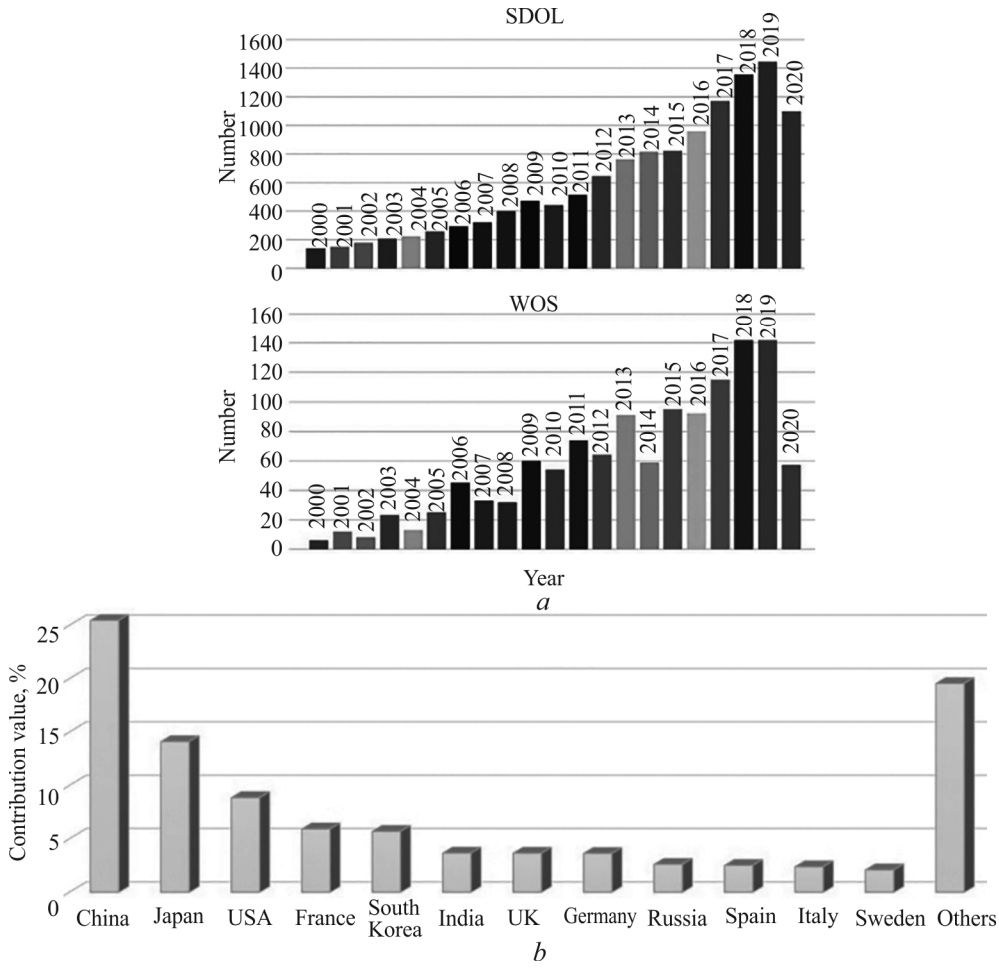

Fig. 1. Research works (*a*) published on the SPS of metal materials (adapted from SDOL and WOS) and relative distribution (*b*) of publications by countries [26]

The SPS technique established initially as a rapid powder consolidation method is used to fabricate various high-property metals, ceramics, polymers, and composite materials challenging to be produced by traditional methods. The increasing importance of SPS in metal powder treatment has also been recognized due to its unique mechanism conducive to controlling powder surface condition, atomic diffusion behavior, phase stability, and accelerating densification of metals and alloys. A detailed review of the published SPS research papers was made in the last two decades, aiming to illustrate the development of the SPS technique in metal structure materials on the national and international levels. The results of statistical analysis on the Science Direct on-Line (SDOL) and Web of Science (WOS), as shown in Fig. 1*a*, demonstrate that the study of SPS for metal materials has become more and more extensive in recent two decades. Moreover, Fig. 1*b* shows the relative distribution of the publications by various countries. Hence, such countries as China, Japan, and the USA have become more active in this research by publishing the most significant number of related articles in recent years, according to the analysis reported in Hu's review paper [26].

The alternative spark plasma sintering method based mainly on traditional powder metallurgy (PM) techniques and featured by much higher flexibility in the powder metallurgy processing parameters has become a widely used processing technique for metal/alloy fabrication due to the ease of operation, high reproducibility, controllable grain size, near net shape capability, accurate control of sintering energy, and low energy consumption. Using the SPS method, a local high-temperature state is generated at the contact point between the particles, resulting in evaporation and melting on the powder surface. The powders are consequently activated and consolidated into near-full-density materials. Due to the advantages of rapid heating, lower sintering times, and

temperatures used during the SPS process, unexpected grain growth can also be effectively inhibited. The refined grain size is responsible for the mechanical properties of metals according to the classical Hall–Petch effect. Therefore, the processing parameters involved in SPS are crucial for optimizing the ductility and strength of metals. The SPS technology has been adopted as a widespread sintering route to acquire excellent sintering properties of the metal materials.

Above all, the application of SPS in metal material synthesis has achieved great success. Their performance also exhibits some advantages compared to those fabricated by other traditional sintering methods. This improvement only refers to the preparation of materials. The related SPS parameters, including electric current, voltage, and SPS pressure, affect the densification of metals and alloys. However, there are still questions about the densification mechanism. These include the effects of the main SPS parameters on the sintering mechanisms, densification behaviors, and materials microstructure and properties. In addition, the specific heating mechanism involved in SPS differs from traditional sintering methods, and the contributions to the densification process shall be determined. In a word, SPS, as a relatively new sintering approach, remains many virgin areas that need to be further examined.

This review mainly focuses on basic principles of the SPS technique, its recent developments, and applications in advanced metal structure materials, including lightweight alloys, stainless steels, high entropy alloys, and other unique metal alloys. In particular, the densification mechanism of metals and alloys during the SPS process will be reviewed in detail.

RECENT DEVELOPMENTS AND BASIC PRINCIPLES OF THE SPS TECHNIQUE

RECENT DEVELOPMENTS

The first mentioning of the "SPS" concept can be traced back to a Great Britain patent in 1906 [27]. Early in 1933, Taylor initiated the idea of using external electric current to assist sintering, defined as "electrical resistance sintering under pressure" [28]. An early resistance sintering (RS) was conducted by applying a direct current on samples without pressure. Then, the first commercially operated SPS machines with punches and dies made from electrically conductive graphite were developed [29]. Researchers from developed countries gradually elaborated this technique due to rapid consolidation, and the corresponding theoretical investigation was subsequently launched. The SPS technique has become more intelligent and flexible, with novel materials applications being developed in specific domains in recent decades. Some new sintering methods or fabricating routes combined with SPS have emerged explosively. The remarkable results developed in these years are introduced as follows.

High-current SPS. Aiming to achieve a higher heating rate and sintering temperature, a more advanced SPS device with a high-dense direct current was developed by researchers. As shown in Fig. 2*a*, the capacitive energy

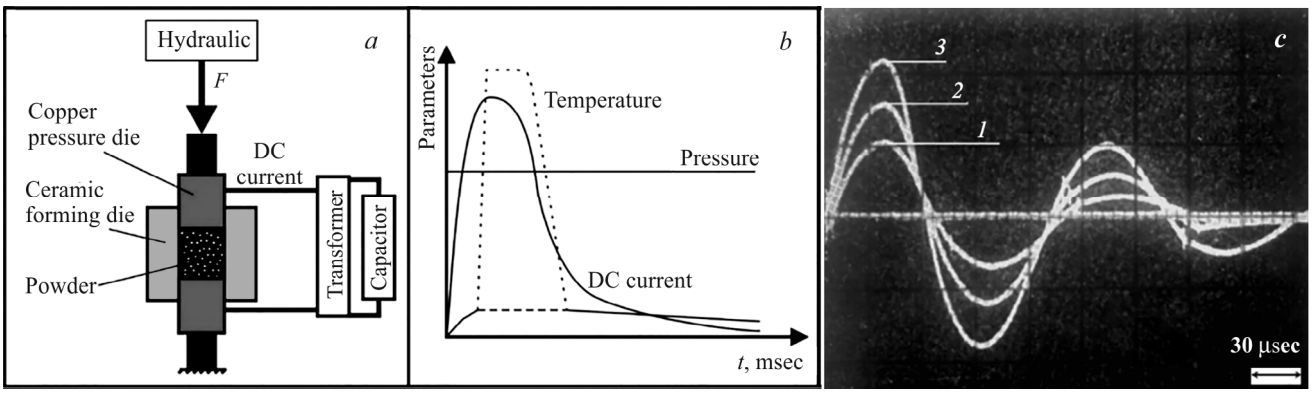

Fig. 2. Flow diagrams of: *a*) action mechanism of the electro-discharge compaction (EDC) system; *b*) essential time-dependent parameters; *c*) pulse current traces and peak currents at 50 (*1*), 80 (*2*), and 110 kA (*3*) [30]

storage system can discharge a high-density current pulse, high-voltage, and low-duration time of each impulse from a capacitor bank through the powders under external pressure. Figures 2*b*, *c* show the essential time-dependent parameters and the typical pulse current traces obtained during the sintering process from the registration system. The peak currents can reach up to 50 (*1*), 80 (*2*), and 110 kA (*3*), respectively [30].

The densification process of nanocrystalline NdFeB powder by electro-discharge sintering (EDS), similar to SPS, was investigated by Lennart Leich et al. [31]. In this work, a large current is discharged from capacitors into a pre-compacted loose powder, thus resulting in complete compaction and excellent mechanical and magnetic properties of the sintered materials. In a study by E.G. Grigoriev et al. [30], the WC–Co and W–Ni–Fe–Co powders were consolidated into solid bulks with respective desirable densities and minimal undesirable microstructural changes due to short consolidation time. Their crystallite sizes were not increased, and the electro-discharge compaction (EDC), a high-voltage (up to 30 kV) discharging, and high-density current (≈100 kA/cm^2) pulse (for less than 300 μsec) were applied simultaneously.

- *High-pressure SPS.* Due to device capacity, the die type and size, and the bearing capacity of the die, the applied pressure in most common SPS during the sintering process is significantly limited. Generally, to obtain a higher pressure, the design and choice of the die become a preferred approach that we usually adopt. Balima et al. [32] developed the 'HP-SPS-Belt' apparatus, as shown in Fig. 3*a*. It is found that the belt apparatus is generally used as a high-pressure generation system. The die assembly is designed to get an optimized tangential stress-strain response inside the die during the loan application. Three binding rings are usually used to strengthen the die, serving for cooling and protection from flying fragments, respectively, during the heating. The HP cell assembly is shown in Fig. 3*b*. The usage of two molybdenum discs ensures good electrical contact. The primary function of the sandwiched mica ring is to keep the die from dangerous overheating via controlling the current path. The pressure that the apparatus can supply to the specimen depends on the die and anvils design. As shown in Fig. 3*c*, the versatility of HP-SPS-Belt in this paper allows it to work at a pressure range from 800 MPa to 6 GPa, and temperatures range from room temperature to 1800°C with 1000 tons of the hydraulic press load.

Compared with conventional high pressure and high-temperature sintering (HP-HT), applying this high-pressure SPS can significantly reduce the phase transition and sintering temperatures. For instance, the transition temperature of alumina lowered to ~500°C from 1 GPa by adjusting and controlling the parameters of this equipment [33]. It is indicated that the density was exceedingly optimized, and the grain growth was also severely inhibited by the HP-SPS sintering.

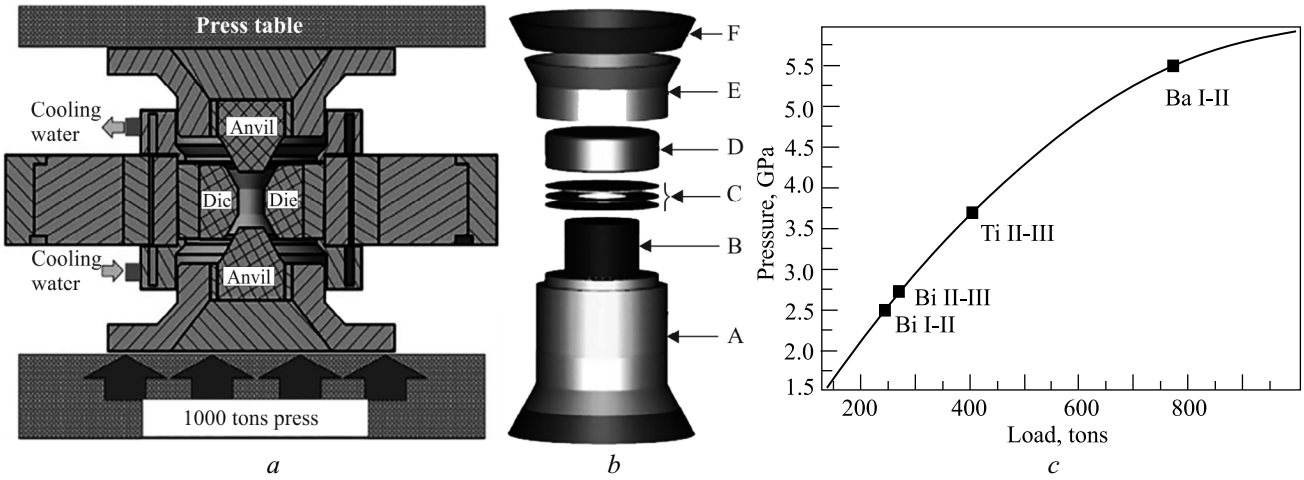

Fig. 3. Flow diagrams of Belt apparatus assembly showing the tungsten carbide anvils and die (*a*); HP cell assembly (*b*): A is fired pyrophyllite tube; B is graphite heater; C is Mo discs sandwiching mica ring; D is steel cover filled with fired pyrophyllite pellet; E is raw pyrophyllite gasket; F is polymer gasket; and pressure calibration curve at room temperature based on electrical transitions of Bi, Ti, and Ba (*c*) [32]

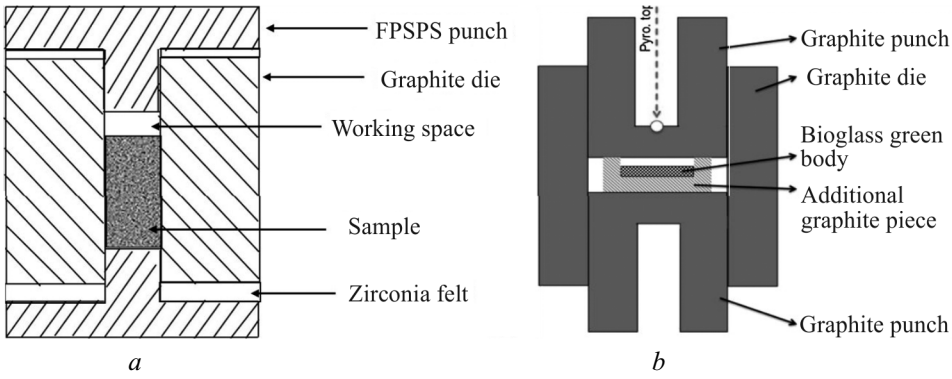

Fig. 4. Flow diagram of FPSPS die designs using (*a*) T-shaped punches [37] and (*b*) additional graphite pieces [38]

- *Pressureless SPS (PSPS).* Pressureless conditions may be required during the SPS process to prepare materials with different properties. This new modification of the conventional SPS approach [34, 35] is usually named free pressure SPS (FPSPS). In the current research, two types of FPSPS die designs used in laboratory experiments and industrial production have been widely accepted: one is the PSPS using modified die-punch assembly, and the other is the PSPS apparatus using additional graphite pieces. Bradbury and Olevsky [36, 37] changed the conventional design assembly to enable a pressureless SPS using graphitic T-shaped punches instead of regular cylindrical punches. Thus, the working space remained constant between the fixed punch faces inside the standard SPS die, resulting in zero external pressure during the sintering process.

The corresponding schematic diagram of the apparatus is given in Fig. 4*a* [37]. Unlike the T-shaped punch described above, another form of PSPS inserted an additional graphite piece inside a regular cylindrical SPS die assembly was developed by Bertolla et al. [38], as depicted in Fig. 4*b*. The height of the built-in piece is higher than that of the green bodies, ensuring the additional structural member was subjected to any minimum applied pressure and prevented it from affecting the sample. Above all, PSPS is an exciting process due to ease of material preparation, controlled multi-step processing, high heating rates, potential electrical effect contributions, in situ synthesis, and net shaping of powder materials. Also, PSPS is widely used for fabricating various materials due to its ability to prevent grain growth due to high heating rates for ensuring enhanced mechanical properties, produce highly porous structures with controlled porosity ratio, and consolidate green powder compact within a short period. Besides, intending to obtain high temperatures and heating rates during the sintering process, graphite paper spacers and zirconia felts are usually used at the contact position to ensure sufficient contact resistance between the punch and the die [38–40].

- *Spark plasma extrusion (SPE).* Despite numerous advantages of standard SPS, there still exist many limitations, for instance, the inability to impose process-induced recrystallization and produce products of complex and extended geometries. In order to solve these problems and use the benefits of recovery and recrystallization for metal materials during hot-deformation, the SPE was invented by combining extrusion with the consolidation of powders simultaneously under the influence of electric current. The SPE process boasts several advantages, including electrically activated dynamic recrystallization. It allows for microstructural refinement, enhanced phase transformation kinetics, and the production of materials with more complex and extended geometries. The schematic diagram of the SPE apparatus is shown in Fig. 5*a* [41]. The powders are initially pressed inside the extrusion container and consolidated under pressure, immediately followed by the extrusion of the material outside the container through the smaller opening in the die. A crowd of regions, including deformation zone (DZ), the dead metal zone (DMZ), are developed inside the container during extrusion and the schematic of extrusion cross-section, showing discard region, extruded region, and corresponding locations (1 to 4), are exhibited in Fig. 5*b*. The SPE has been successfully applied to fabricate metals and alloys, and some composites. The extruded products with high density, simultaneously characterized by few cracks, exhibits unique microstructures and excellent performances [42].

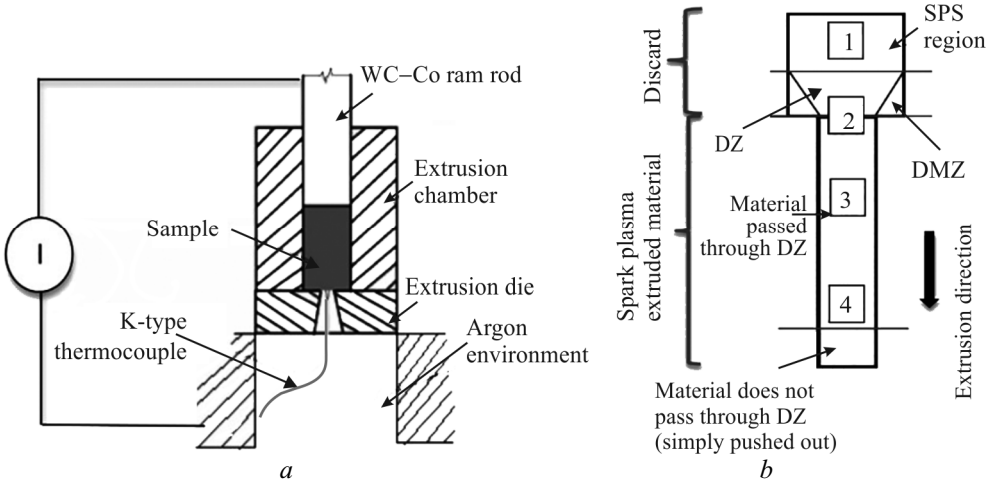

Fig. 5. Flow diagram of (*a*) SPE setup and (*b*) extrusion cross-section, showing discard region, extruded region, and locations from 1 to 4 [41]

- *Spark plasma welding (SPW).* To our best knowledge, the primary application of SPS is to consolidate powders into a dense bulk. At the same time, some researchers use it as a resistance joining method to weld two the same/different metal parts together. In Jinhua Yang et al.' work [43], joining 316L stainless steel rods with or without a powder interlayer was successfully carried out using spark plasma sintering equipment. As schematically shown in Fig. 6*b*, two rods were placed abutted against each other, sandwiched between copper spacers and graphite spacers. Between the two rods, a layer of stainless steel powders acting as an effective local heat source during the welding process due to the higher electrical resistance than the bulk material measured by the 4-wire measure method, as shown in Fig. 6*a* was added. The results indicated that high-strength joint could be obtained, especially by rightly adjusting current and heating time. Three kinds of aluminum/stainless steel (Al/SUS) clads were produced using the modified SPS apparatus shown in Fig. 6*c* and reported in the research paper [44]. It is indicated that the production of Al/SUS clad composite materials under the powder/bulk condition could be very helpful to form a stronger bond.
- *Flash spark plasma sintering (FSPS).* Based on a mature commercial SPS platform, the FSPS was developed, and the apparatus is shown as Fig. 7 [45]. The samples are usually cylindrical, and it is directly connected to the electrode through the punch. In FSPS, rapid heating rates were adopted, and uniaxial pressure is

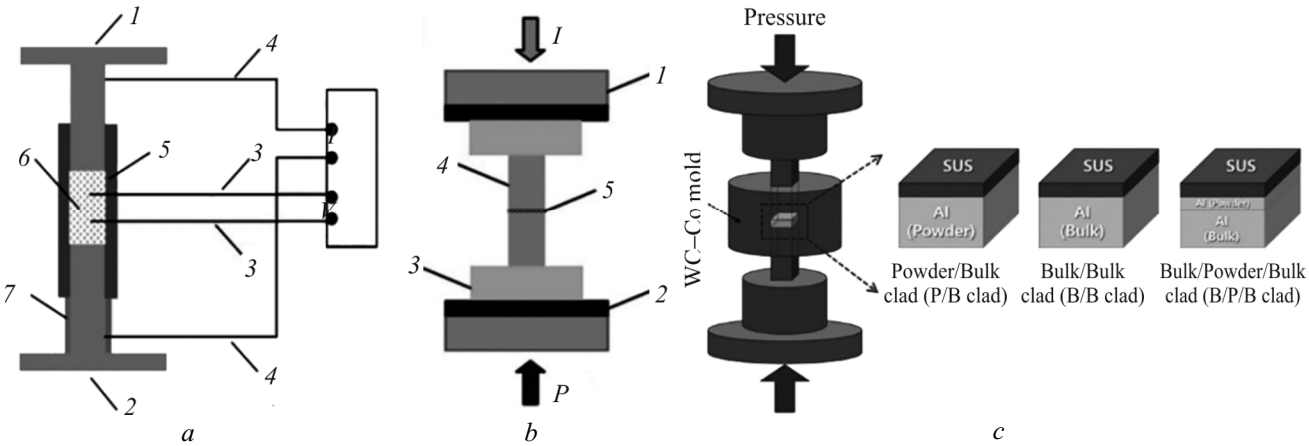

Fig. 6. Schematic drawing of the (*a*) resistance measurement device: *1*) upper piston, *2*) lower piston, *3*) voltage probes, *4*) current probes, *5*) steel tube (inner diameter 10 mm), *6*) powder, and *7*) plastic fixing tube; (*b*) the SPS set-up: *1*) electrode, *2*) graphite spacer, *3*) copper spacer, *4*) 316L stainless steel rod, and 5) 316L stainless steel powder [43]; and (*c*) 3 kinds of aluminum/stainless steel clads [44]

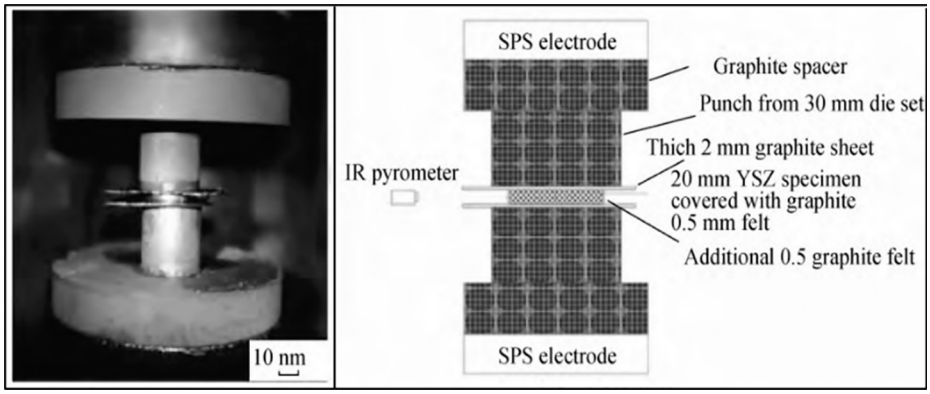

Fig. 7. The photo and schematic drawing of the FSPS platform [45]

also applied simultaneously to promote sintering densification. Compared with traditional SPS, the high-current is directly applied to the compact without an additional high electric field to heat the sample in the FSPS. The advantages of the FSPS can be briefly summed up as follows:

1) The sinter's driving force is significantly improved due to a direct application of uniaxial pressure on the sample, resulting in rapid densification.

2) The contact area between the FSPS electrode and sample is more significant, which is beneficial to fabricating bulk materials with desired densification and uniform microstructure.

In Francesco Gucci's research work [46], $TiNiCu_{0.05}Sn$ was sintered using a new hybrid Flash-SPS (FSPS). It is revealed that the high heating rate ($7700°C \cdot min^{-1}$) can be achieved, finally producing almost single-phase samples with relatively high density. The sample sintered at 1040°C showed a higher power factor and a lower thermal conductivity than the sample sintered by conventional SPS, resulting in a higher ZT at 350°C.

Except for the above developed SPS technologies or routes, there is no doubt that more advanced SPS methods will be developed shortly to obtain bulk materials with larger size and better performance. Here, some designs and propositions for the SPS technique will be given as follows. Aiming to realize the synthesis of larger bulk materials with a more uniform microstructure, the SPS apparatus equipped with double/multiple pulses DC generators can provide various currents with different current densities and frequencies from another direction to the sample be developed.

With the development of proposed genetic engineering, high-through preparation and analysis have become a hot research issue for many material researchers in recent years. Based on the advantages of the SPS in materials preparation, the SPS apparatus, which can produce many products or a series of samples in one sintering process, becomes an up-and-coming technique. Based on this novel idea, the die design becomes an effective way to realize the high-through preparation of materials. In the book [47], the dies with samples assembled by parallel configuration and serial-multiple parts configurations with or without intermediate spacer, as shown in Figs. 8*a*, *b*

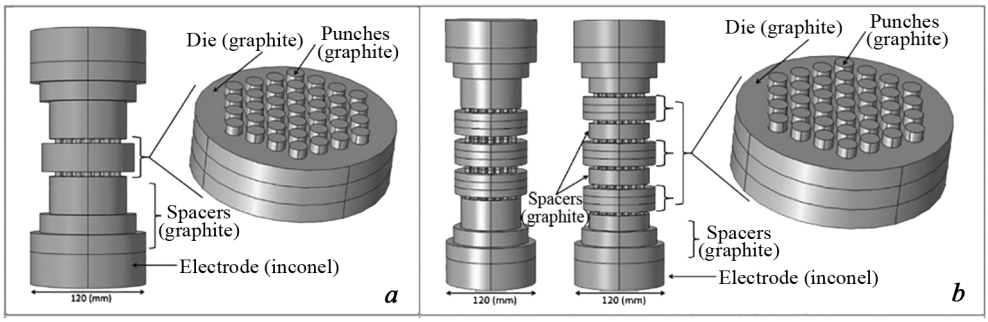

Fig. 8. Samples in (*a*) parallel configuration and (*b*) serial-parallel multiple part configuration with or without intermediate spacer [47]

were first introduced. If this idea comes true, the product-development cycle of new materials will be seriously shorted, inevitably resulting in a significant improvement of the new material industry. Though the above new concepts and ideas are still embryonic, they are all educated guesses and are believed to be a reality soon.

BASIC PRINCIPLES OF THE SPS TECHNIQUE

A detailed description of the fundamental process of SPS has been given in many published papers. Here, a brief introduction to the SPS will be made. The SPS apparatus, consisting of a mechanical loading system, a DC pulse current generator, atmosphere/vacuum apparatus, a water-cooling system, and a data acquisition system, is schematically illustrated as Fig. 9*a* [48]. The powders are initially poured into a predesigned die. In the following high-temperature sintering process, a vacuum or protective gas is utilized as a sintering atmosphere to avoid oxidation, especially metal materials. Then, the electric current flows through the die via punch shown in Fig. 9*b*, with an axial pressure applied meanwhile [49]. During this process, the electric current passes through the die and conductive sample, heating the die and sample due to the resistance of the contacts between powder particles, graphite foils, and graphite spaces. In addition, the plasma between particles generated by the applied pulse DC will cause the self-heating of powders due to the joule-heat effect.

Moreover, local high temperature at the powder contacts can be produced due to the appearance of plasma, resulting in a functional movement of contaminations and the following enhancement of powder surface activation, formation of the neck at contact points, atomic diffusion, and plastic flow. Joule heating and plastic deformation

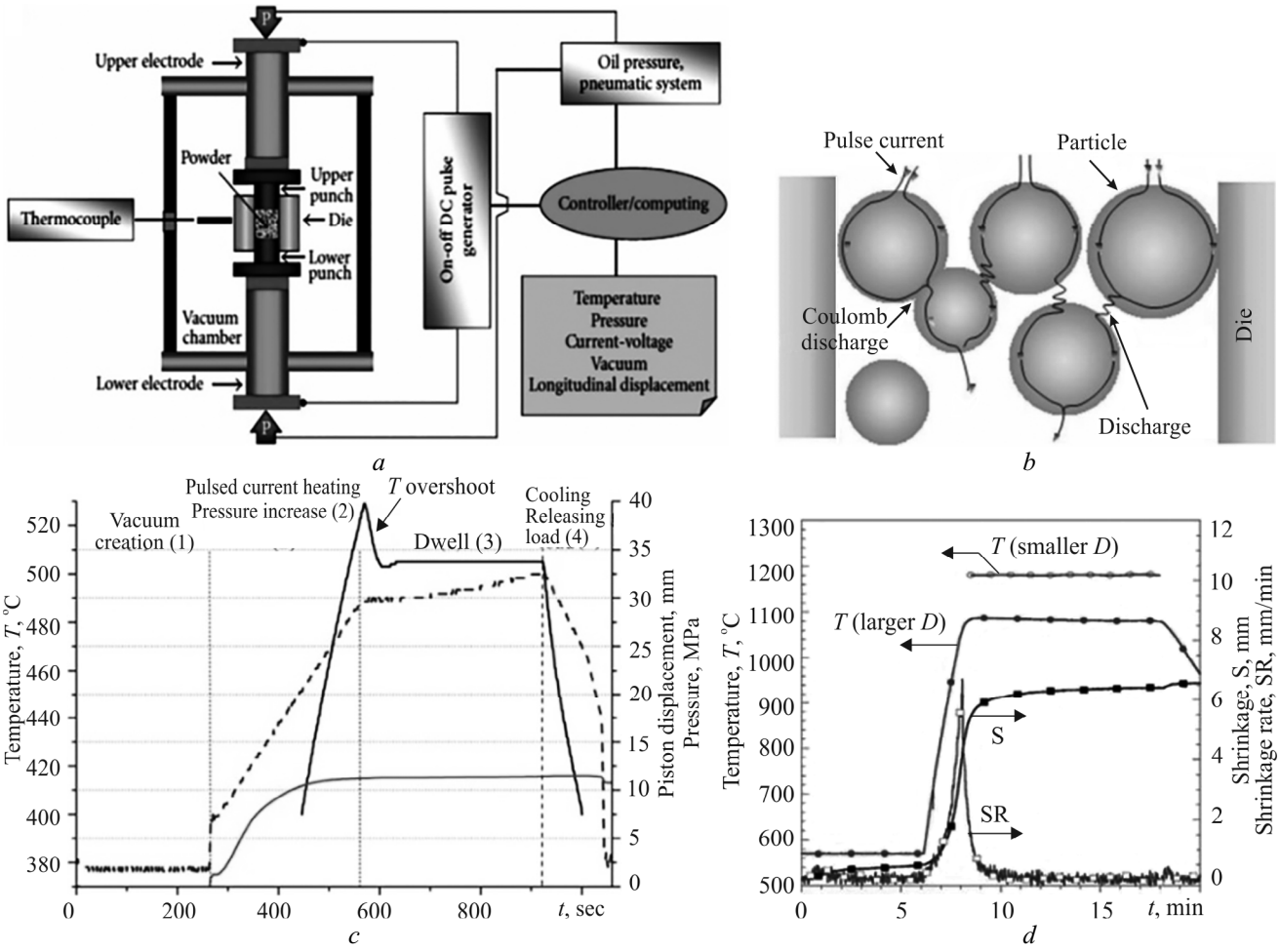

Fig. 9. Flow diagram of SPS process (*a*) and pulse current flow among powder particles (*b*), the temperature, pressure, and piston displacement with time in four consecutive stages (*c*), and the temperature, sample shrinkage, and shrinkage rate profiles (*d*) [3, 48–50]

effects also enhance densification of the sintering, leading to improved sintering efficiency and restriction of grain growth. Besides, the water-cooled chamber can efficiently reduce the furnace temperature and improve the cooling rates after sintering. These features will cause an inevitable advantage and fast heating and cooling rates, making it possible for the SPS to consolidate the powders into a dense bulk at low sintering temperatures, shorter sintering times, and soaking times. As shown in Fig. 9*c* [3], the corresponding sintering data such as temperature, pressure, and displacement are collected directly and automatically by a computer during the whole sintering process. The corresponding displacement rate of the sample can also be indirectly obtained according to the first derivative of the displacement versus time, as Fig. 9*d* shows [50]. Also, the resistance variation of the powder compact during the sintering process can be well traced according to Ohm's law based on the directly collected current and the resulting voltage. It is very beneficial to understand the densification mechanism of the materials by analyzing these data obtained in real during the whole SPS process.

ADVANCED MECHANISMS INVOLVED IN SPS

Densification is one of the most significant characteristics of materials influencing their physical and mechanical properties. There is no doubt that densification will significantly enhance physical and mechanical properties simultaneously for metals and alloys. In the last section, all SPS parameters have been introduced in general, and they all affect densification. In the following section, the effects will be investigated in detail.

SPS ELECTRIC CURRENT OR ELECTRIC FIELD

It is known that SPS differes from other traditional sintering methods through applying pulse current during SPS. Most of the outstanding advantages involved in the SPS technique have been proved to be directly or indirectly associated with electric current [51]. Electric current can increase the mass transformation by increasing point defect concentration and decreasing the activation energy for defect migration [52, 53]. In a word, increasing SPS electric current enhances the densification of metals or alloys due to better mass transportation. Owning a high heating rate is the most significant and obvious benefit induced by electric current. The current types applied widely in the modern SPS devices are mainly pulsed DC, according to the statistical results conducted by Hu [26]. It is widely accepted that the heat generation mechanism is joule heat caused by the resistances of the material system to electric current [54]. The whole resistances mainly include inter-particle contacts, die, graphite foil-powder contacts, and punches. It is reported that the resistances of graphite foil-powder contacts account for a large proportion (~64%) of the total resistance except for the resistance of powder compact in Chawake's work [55].

When conductive metal materials are consolidated via SPS, the pulsed current will directly flow through the powders and the die. In the initial sintering stages, the measured resistance of the sample can be significantly higher than the intrinsic resistance of conductive materials due to the contribution from the contacts among the numerous inter-particles covered with a thin layer of oxide or impurities [56]. In this stage, Joule heating is primarily triggered by the high-density current due to the inter-particle contacts and concentrated in the grain boundary region, facilitating the joining of the powder particles [57]. Because of the collapse and closure of the pores, the inter-particle contacts will gradually diminish with the increasing densification of the sintering materials. According to the investigation [55], the resistance of the sintered conductive material will ultimately reach the saturation state at ~0.3 Tm, after which the primary heating source will be changed.

It is revealed that in some recent studies, the indirect thermal effect and electrical effect associated with pulsed current also have significant influences on the densification behaviors of the sintered materials during the SPS process and further affect their structure and properties [58, 59]. The relevant effects can be summarized into the following *four aspects*.

- *Surface conditions.* The electrical discharge and high-temperature plasma are commonly believed to appear during SPS [60], which can effectively destroy or remove the adsorptive gas, oxide layer, and any contaminants on the particle surface, resulting in an activation and purification effect of particles and consequently a promoting densification process of the sintered materials [17]. M. Tokita presented a comprehensive description of high-temperature plasma characteristics and formation mechanism during the SPS in 1999 [61]. It is clarified that the

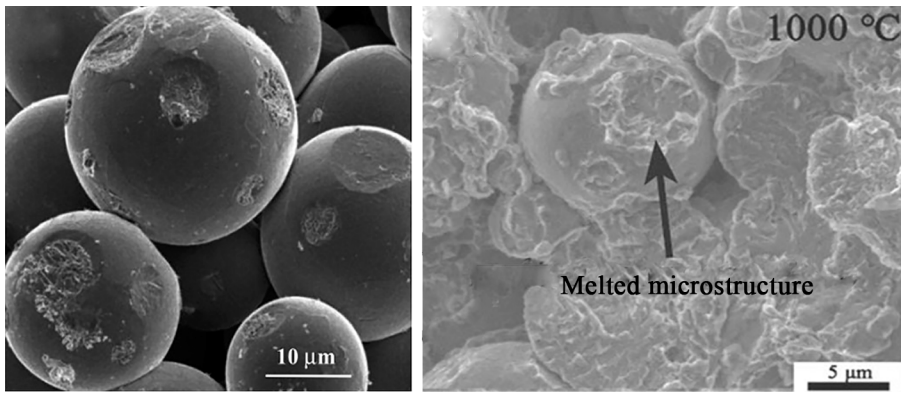

a *b*

Fig. 10. The fracture surface of (*a*) $Ti_5Al_{2.5}Fe$ alloy produced by PSPS [40] and (*b*) nickel alloy powders processed by SPS [62]

spark discharges would emerge in the gaps among the powder particles under an appropriate condition in the SPS process, which immediately led to a local high-temperature (several thousands of degrees centigrade). The local high temperature generated by spark plasmas could cause local melting and evaporation on the powder particles' surfaces, which was observed by Yamanoglu et al. [40] for a $Ti_5Al_{2.5}Fe$ alloy during the PSPS process and Zhiqiang Fu for $Fe_{25}Ni_{25}Co_{25}Ti_{15}Al_{10}$ high-entropy alloy [62], as shown in Fig. 10.

For this reason, better sintering necks can be created, accelerating the densification of the sintered materials. According to the two investigations conducted by Nagae et al. and S. Suzuki et al., the surface films of aluminum and WC powders are ruptured through the local high-temperature induced by the spark plasma created in the gaps. The spark plasma also leaves discharge patterns on insulators [63]. As the plasma generation site is limited, the plasma is concentrated only on the melted area and leaves some patterns on the surface of the sintered samples.

Hence, the etched area is localized. It is clarified that superficial surfaces of polyethylene are etched by spark plasma in a short period, as depicted in Fig. 11 [64].

- *Atom diffusion.* In general, interface reaction is regarded as the minimal scaled dynamics behavior during the SPS process, by which the discrete particles evolve into a dense metallic part. Most researchers believe that various materials' rapid densification and outstanding SPS performance may correlate with atomic diffusion under the complex conditions of the press, temperature, pulsed DC, and electromagnetic field [65]. Li et al. studied the atomic diffusion behavior related to an Al–Fe powder contact. They found that the inter-diffusion coefficient under the condition of pulse current was approximately 46 times higher than that without pulse current at 600°C, despite an increase in the diffusion activation energy.

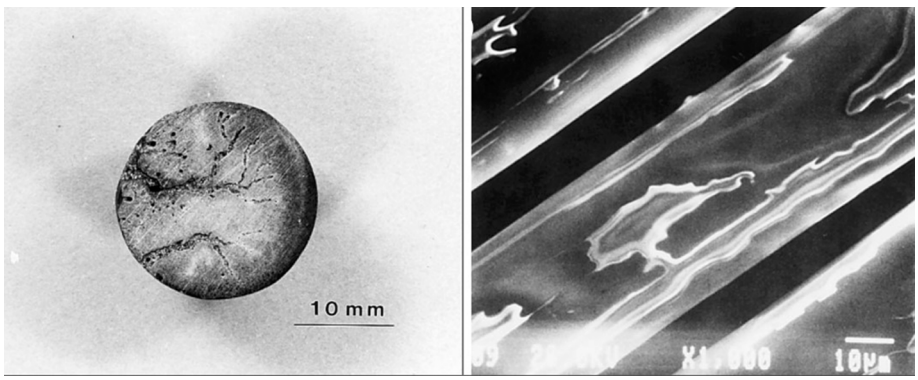

a *b*

Fig. 11. Electric discharge pattern on the surface of $CeSiNO_2$ (*a*) and SEM image (*b*) of the polyethylene fiber exposed to electrical discharge in the air [64]

- *Flow stress.* Small vibrations in the forming load were inevitably produced during the sintering process, resulting in the momentary softening phenomenon. According to classical electro-plasticity theory, the electric current can lower the material's flow stress by facilitating the dislocation movement and reducing the electrochemical potential of the rate-limiting vacancies in the space charge clouds near grain boundaries. Consequently, it helps realize rapid consolidation of powder materials during the SPS process [66, 67].
- *Solid-state phase transformations.* Phase transformation is an essential factor affecting the densification behavior of metals and alloys in the sintering process. These effects on solid-phase transformations induced by the electric current can be classified as accelerating or retarding action. The effects depend not only on the compositions and prior treatments of the raw materials but also on the current density and frequency [68]. As it is known, partial melting of metal materials during SPS at high temperatures is a type of phase transformation. This phenomenon may result in enhanced or reduced densification of the sintered materials.

The W–5.6Ni–1.4Fe heavy alloys were fabricated using the SPS method with subsequent examination of densification and grain growth. It is found that the formation of a liquid phase in heavy tungsten alloys (WHAs) results in higher densifications at elevated SPS temperatures due to improved wetting ability of the liquid phases and enhancement in diffusion [69]. Contrarily, a de-wetting phenomenon occurred in the Cu–Pb system at specific SPS temperatures and, hence, decreased the alloys densification. Empl et al. [70] reported that the liquid Pb does not wet Cu grains when the sintering temperature exceeds 400°C. Xie [71] consolidated gas atomized $Al_{0.7}CoCrFeNi$ powder using the SPS method and investigated the effect of phase transformation on its properties and densification kinetics during the sintering. The main conclusion is that the BCC-to-FCC phase transformation causes a grain size reduction and ductility enhancement and hinders the densification process due to decreased diffusion coefficients.

SPS TEMPERATURE

Similar to other traditional sintering methods, incremental changes in SPS temperature commonly bring about higher relative density for the materials. Such an enhancement in metals and alloys is mainly due to increasing inter-particle contacts and decreasing the pores between metal particles because of the elevated grain growth at higher SPS temperatures [72]. In addition, better necks can be formed between metallic and alloyed particles due to high SPS temperatures. Faster diffusion processes and high plastic flow rates have also resulted from high SPS temperatures [73]. Besides, an increment in SPS temperature decreases the strength of metallic powders, which enhances the creep flow [13]. Such a trend can be found in Al-2024 fabricated by the SPS method [74]. In addition to the above reasons, the viscosity in metals or alloys and phase transformation are also critical factors that can alter the effect of SPS temperature on the densification behavior. The $Cu_{47}Ti_{33}Zr_{11}Ni_6Sn_2Si_1$ alloy spark plasma sintered at higher temperatures obtained better densification due to lowered viscosity at such temperatures [75]. On incrementing SPS temperature by more than 890°C, phase transformation occurred for titanium and its microstructure changes from α (HCP) to β (BCC), which resulted in higher densification due to more space for diffusion in the β-phase [76].

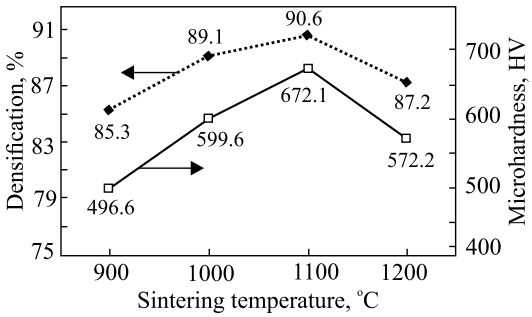

Fig. 12. Effect of sintering temperature variation on the densification and microhardness of Fe–18Cr–2Si alloy [77]

On the other hand, excessive sintering temperature will induce crystal grains to grow up and cracks to produce, finally leading to a reduced bending strength of the sintered materials, which is not beneficial to the performance improvement. The densification trend first increased and then decreased with an increase in sintering temperature in Fig. 12 for the Fe–18Cr–2Si alloy [77]. The decrease in density with a further increase in sintering temperature may be caused by partial melting of particles surfaces, which might have occurred at this temperature.

SPS PRESSURE

Generally speaking, increasing the uniaxial pressure during the SPS process can make sintering easier and result in a higher relative density of metals and alloys due to SPS pressure's mechanical and intrinsic effect [78]. First, increase in pressure can effectively decrease the gaps among powder particles, enhancing diffusion during the sintering. Next, a better flow and breakage of agglomerated particles could be produced based on this increased pressure. The following particle rearrangement and plastic deformation of powders can be generated, which results in an effective decrease of the pore size and increase of contact area between particles, leading to limited grain growth, weakening of metallic powders, and better final densification [79].

Additionally, increasing uniaxial pressure can also effectively decrease sintering temperature, which some research works have confirmed. The intrinsic effect of the SPS pressure is referred to increase in diffusion driving force [80], induced by these mechanical effects.

SPS TIME

It is generally accepted that the incremental changes in SPS time usually enhance the densification of metals and alloys due to enhanced mass transfer, improved inter-particle bonding, reduced porosities, and enhanced heat flux [77, 81, 82]. During the sintering process, the coalescence and closure of intergranular pores occurred because of incremental changes in SPS time, resulting in enhanced densification and expanded grains for the sintered metals [83]. Moreover, prolonging SPS dwell time can significantly decrease the viscosity of metal powders and induce some additional structural relaxations, leading to an enhancement in the density of sintered metals.

Contrarily, the incremental change in SPS time may negatively affect the density of metallic systems. It is revealed that the gradual changes in SPS time of more than 10 min do not affect the densification of M2 steel [84]. In such a system, prolonging the sintering time did not further increase the densification of the materials because high SPS pressure may have brought about the maximum densification of the system at early times of sintering. Moreover, some studies have reported a reduction in densification at high SPS dwell times. For instance, it was observed that the incremental changes in SPS dwell time slightly degrades the densification of pure copper due to expansion and obturation of the gases absorbed on the surface of Cu powders during the plastic deformation in the early stage of the sintering [24].

SPS HEATING RATE

For different metallic systems, positive or negative effects on the densification of metals and alloys can also be caused by the incremental changes in SPS heating rate. Generally, increasing heating rate reduces the relative density of sintered materials because the materials can acquire longer sintering time in lower heating rates, resulting in better densification. Moreover, large quantities of local "hot spots" will be formed at a high heating rate, which causes local melting via arcing and immature necking. This phenomenon results in entrapments of porosities and lower densification of the sintered materials [85]. Additionally, due to not enough time for neck formation at an early stage of sintering at higher heating rates, premature necking and non-homogenization may also be generated [86].

Hu [87] investigated the densification and microstructure evolution during the SPS consolidation process in the W–Ni–Fe system. It is revealed that diffusion is more sufficient in the slow-heated SPS process, but fast heating helps maintain relatively small grain sizes. On the other hand, a higher heating rate may result in higher densification because of generating better surface activation and neck formation between powders. Moreover, sintered samples with higher heating rates that experience higher temperatures at the early stages of SPS may enhance their densification [79].

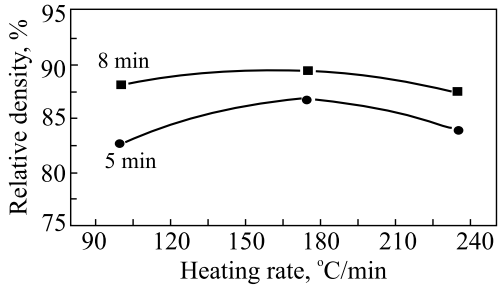

Fig. 13. Effect of heating rate on the relative density of nickel alloy processed by spark plasma sintering [88]

The heating rate also has both simultaneous reduction and incremental effects on the relative density of metals. For instance, increasing the heating rate up to a specific value would increase the relative density. However, further increasing the heating rate decreases relative density. The relative density of nickel alloys was first raised by reducing the amount and size of the porosities when the heating rate increased to 175°C · min^{-1}. However, the density decreased when the heating rate was further increased to 235 °C · min^{-1}, as shown in Fig. 13 [88].

ADVANCED METAL STRUCTURE MATERIALS

In order to sinter these hard-to-sinter materials such as refractory metals and special ceramics with excellent performances, the early SPS equipment was invented. However, the performances of the prepared materials did not show significant improvement without applying conventional pressure and sintering simultaneously. Hence, many relevant researchers devoted themselves to pay attention to updating the SPS technique now available and developing its further applications. The modern SPS devices are suitable for fabricating the above materials and more suitable for synthesizing novel metal materials, such as high-quality special steels, novel lightweight alloy materials with high performances, high entropy alloys, and other metal alloys. Recently published papers have shown the success of SPS for preparing these materials, and the developed materials also exhibited excellent performances. In this section, some representative examples of applying SPS in every material system are illustrated in detail.

HIGH-QUALITY SPECIAL STEELS

Generally, high-quality special steels refer to these steels with particular chemical composition, preparation technology, and microstructure. These properties can be used in aeronautics and astronautics, marine development, and weapon facture. The development of these steels directly reflects the level of modern technology and industrialization of a country. These steels are usually prepared by a double vacuum smelting process, in which an ultra-clean environment is needed. It is believed that the whole preparation process is quite complex, challenging, and energy-intensive, which severely restricts their application and further development. Thus, the newly developed SPS technique is gradually adopted to achieve fully dense bulk materials at low temperatures with short heating, soaking, and cooling times.

Oxide dispersion-strengthened (ODS) steel as a candidate material used in the nuclear power industry, especially for the first wall cladding material and high-temperature structural material has received more and more attention from researchers because of its excellent mechanical properties, high-temperature stability, and radiation resistance. The most common processing routes used to sinter ODS steels are hot extrusion (HE) and hot isostatic pressing (HIP). It is found that compacted with HIP, the tensile strength and hardness of ODS steel after HE are higher, and the dispersion distribution of oxide strengthened phase is more uniform [89]. However, spark plasma sintering has been reported as a promising process to better tailor a suitable bimodal grain structure in the last years.

David Pazos et al. made a microstructural comparison of oxide dispersion strengthened Fe–14Cr steels produced by HIP followed by hot deformation and SPS. It is concluded that the relative density reaches up to

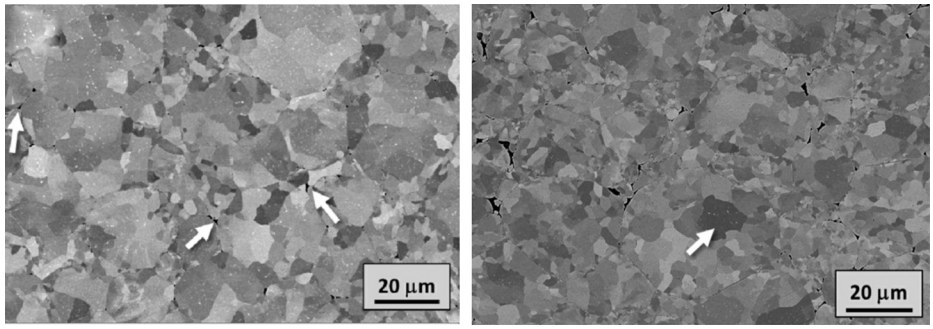

a *b*

Fig. 14. SEM detailed microstructure of samples consolidated by (*a*) HIP at 900°C, 140 MPa and (*b*) SPS at 1000°C, 80 MPa [90]

99.5%, and the finer microstructures of the material consolidated by SPS are produced compared to HIP consolidation, as shown in Fig. 14 [90].

The Fe–14Cr–5Al–3W–0.4Ti–0.25Y_2O_3 oxide dispersion-strengthened (ODS) steel [91] was consolidated by SPS using sintering temperature (1100°C), compacting pressure (80 MPa), heating rates (100 and 400°C · min^{-1}), and dwelling time (5 min). It is revealed that non-textured bimodal microstructures composed of micrometric and ultrafine grains were obtained. A higher percentage of Zr nano-oxides and larger regions of ultrafine grains were produced due to the increase in Zr content, as shown in Fig. 15. Additionally, the ultrafine grains also were prone to be promoted by higher heating rates. Besides, the undesirable growth of the nano-oxides and the austenitic grains can be partially avoided during the sintering stage because of the rapid heating and short dwell time. Subsequently, a ferrite transformation occurs during the cooling process. Higher densification was also caused by the fast generation of internal heat increases. Based on the pinning effect of the dislocations, improved densification, and the refined microstructure, the strength of the sintered products was significantly increased.

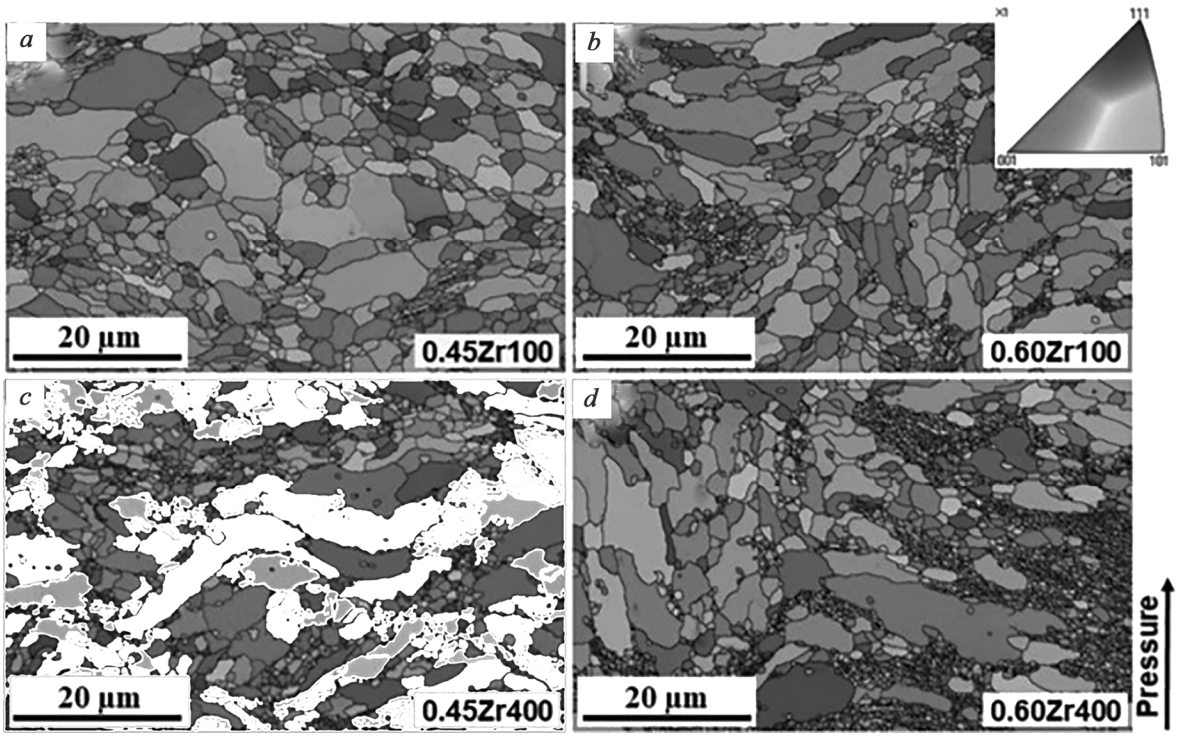

Fig. 15. ODS–0.45Zr100 (*a*) and ODS–0.60Zr100 (*b*) sintered at 100°C · min^{-1}, ODS–0.45Zr400 (*c*) and ODS–0.60Zr400 (*d*) sintered at 400°C · min^{-1} [91]

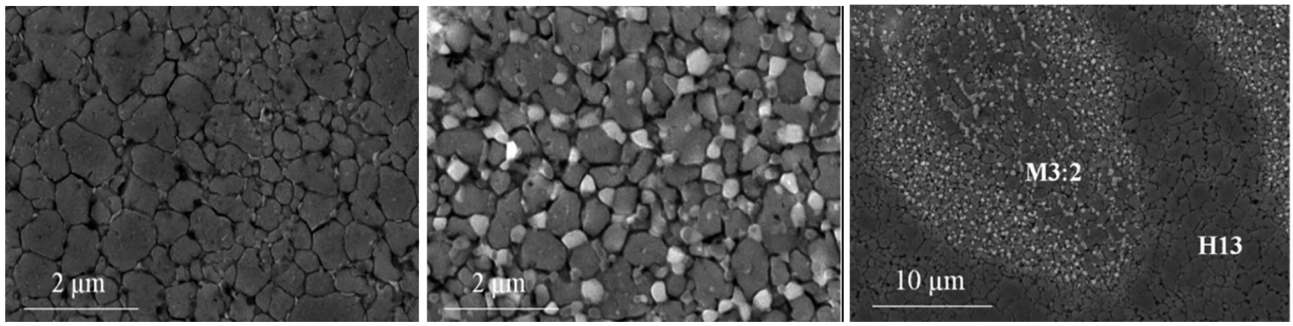

a *b* *c*

Fig. 16. Microstructure of three steel types obtained by SPS: *a*) H13; *b*) M3:2; *c*) hybrid tool steel showing the H13 and M3:2 regions [92]

Tool steels, such as hot work tool steels and high-speed steels, both require a proper compromise between hardness and toughness to provide high wear resistance and adequate resistance to cracking. The possibility to produce hybrid materials with tailored properties has been first proposed to reinforce the metal matrix with more complex steel as a valuable solution to overcome this problem. Using spark plasma sintering, hot work tool steel (AISI H13) and high-speed steel (AISI M3:2) powders were successfully co-sintered to produce hybrid tool steels with near full density samples (>99.5%) and very fine and homogeneous microstructure, as shown in Fig. 16 [92].

STAINLESS STEEL

Due to unique corrosion and mechanical properties, stainless steel, an essential iron-based alloy, has found widespread applications in some particular fields such as aerospace, automobile, recreational, and chemical processing [93, 94]. Aiming to protect stainless steel from chemical attack, a minimum of 10.5% chromium (Cr) in stainless steel must be required. Other alloying elements such as Ni, Mn, Mo, Nb, and Ti, also significantly affect the properties of the stainless steel. The most modern stainless steels can be fabricated by powder metallurgy routes such as hot isostatic pressing, high-temperature high pressure, and recently developed spark plasma sintering. Compared with wrought stainless steels, carbon composition is slightly lower in sintered stainless steels, causing an enhancement of ductility and formability [95].

Among all the PM routes, the SPS process has been gradually applied to fabricate stainless steel due to its unique operating conditions and processing advantages, and significant achievements have been achieved. In work [81], SPS sintered 316L stainless steel obtain the ultrafine-grained microstructure, resulting in a significant increase of strength and hardness. Besides, as the sintering temperature increased, the higher relative density of the SPS 316L stainless steel can be produced. It is revealed that in research [96], a remarkable increase in densification duplex and ferritic steels can be observed. In the A. Almathami et al.' study, three austenitic stainless plates of steel with different Al content were successfully prepared through a combination of cryo-milling and spark plasma sintering. It was revealed that the SPS process was found to minimally influence the FCC recovery because the supplied energy was insufficient to overcome the activation energy governing the rearrangement of dislocations required to complete the FCC recovery [97].

In another work [98], pure nanostructured ferritic steel alloy (NFA) and SiC–NFA composite samples with nearly complete density were obtained via SPS sintering at only 950–1000°C. It can be concluded that the sintering temperature can enhance the densification of the nanostructured NFA and SiC–NFA composites. Besides, SiC addition delays γ-Fe formation from α-Fe during the SPS process. S.R. Oke et al. [99] fabricated duplex stainless steel (SAF 2205) reinforced with TiN nanoparticles using optimized SPS sintering parameters of 1150°C, 10 min, and $100°C \cdot min^{-1}$. As shown in Fig. 17, the variation of displacement and shrinkage rates revealed that three densification stages relating to micro-nano particles rearrangement, localized plastic deformation, and rapid densification were observed during the SPS process.

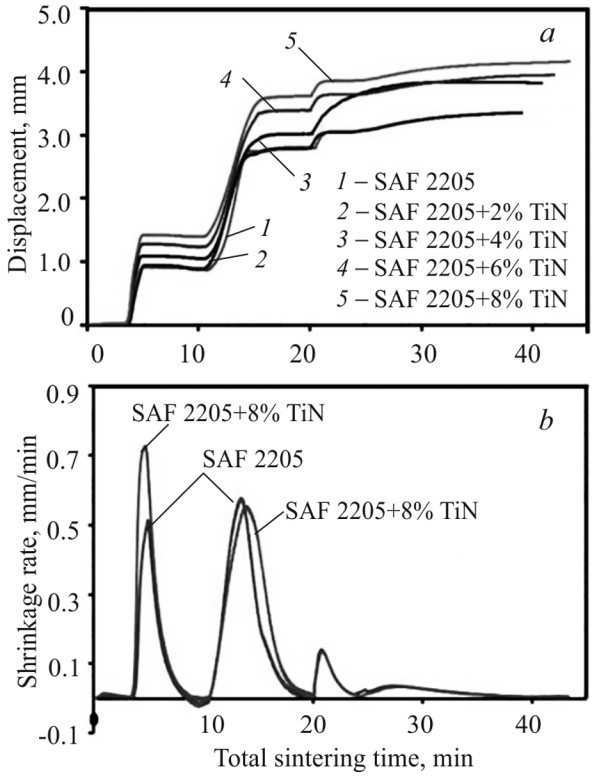

Fig. 17. Variation of punch displacement (*a*) and shrinkage rate (*b*) with total sintering time for the SAF 2205 reinforced with TiN nanoparticles [99]

NOVEL LIGHT ALLOY MATERIALS

As the basic technology of aerospace manufacturing, the applications and prototyping of light alloy materials including Ti, Al, Mg, and other metal alloys are becoming more and more extensive. With the maturity and constant improvement of research and development of lightweight alloys with high performance, the forming technique is also developing rapidly towards the direction of large-scale integration and complexity at home and abroad. The SPS technique has become an effective and rapid fabrication method for these lightweight alloys due to its distinguishing sintering features.

TITANIUM AND TITANIUM ALLOYS

Due to its excellent performance, such as low density, high strength, good corrosion resistance, and good biocompatibility, titanium and its alloys are widely used in aerospace, automobile and ship, biological medicine, and other fields. With the increasing requirements of lightweight materials for weapons and equipment, the development of titanium and titanium alloys has become an essential part of national strategic development. As the most potential preparation method, powder metallurgy preparation technology, especially the novel SPS technique of titanium alloy, has attracted much attention.

The physical and mechanical properties of spark plasma sintered pure Ti and Ti–TiB_2 composite was investigated as a function of TiB_2 concentration and sintering temperature by Mohammadzadeh [100]. It was concluded that the sintering temperature has the most pronounced effect on the sintered density, porosity, and microhardness. The strengthening effect of the materials was caused by introducing TiB_2, acting as a grain growth inhibitor, subsequently resulting in refined microstructure and in-situ formation of TiB needle-like phases. In Li et al.' study [101], the bimodal Ti–*x*Bi alloys were fabricated using mechanical alloying (MA) and spark plasma sintering from elemental powders. Ti–0.5Bi alloy exhibited excellent comprehensive mechanical properties with high compressive strength and ductility attributed to the typical bimodal structure comprised of coarse grains

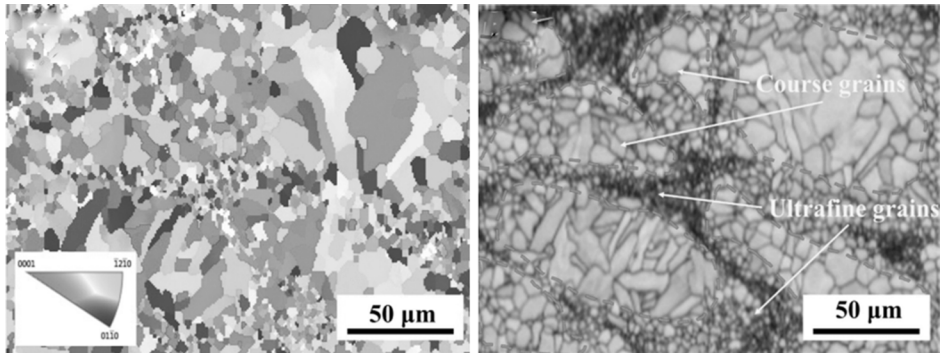

a *b*

Fig. 18. EBSD images depicting the bimodal microstructure of the Ti–0.5Bi alloy: *a*) IPF-X map; *b*) image quality map [101]

(CG) and ultrafine grains (UFG) region, as depicted in Fig. 18. According to the Hall–Petch formula, the UFG region contributed tothe high strength while the CG region offered good ductility. The results mean that the controlled MA and SPS technique can effectively tailor the microstructure and propose a promising route to improve the comprehensive mechanical properties of the materials. Ojo Jeremiah Akinribide et al. produced Ti $(C_{0.9}, N_{0.1})$ composites using spark plasma sintering with 0.5 and 1.0 wt.% of graphite addition [102]. The maximum average Vickers microhardness and toughness value of the 1.0 wt.% graphite composite was 24.32 GPa and 45 ± 3.4 J · m^{-2}, respectively. It was mainly attributed to a pronounced grain refinement effect of 1.0 wt.% graphite addition, the presence of the ceramic agglomerates and graphite inclusions and relative more amounts of Ti $(C_{0.9}, N_{0.1})$–1.0 wt.% Gr solid solution.

Spark plasma sintering technology was also used to consolidate Ti–Ta–Ru powders. The effects of sintering parameters on the sintered compacts densification, corrosion, and wear performance were subsequently investigated. Results showed that the addition of Ta with a small amount of Ru significantly influenced the densification, hardness, and corrosion behavior of the sintered alloy. When 9 and 1 vol.% Ru were added, the sintered density and hardness were 92.07% and 330 $HV_{0.1}$, respectively [103]. Ultrafine grained Ti–Cu alloys were fabricated using a combination of high-energy ball milling and SPS [104]. The spark plasma sintered bulk $Ti_{95}Cu_5$ alloy was composed of Ti_2Cu precipitates uniformly distributed in an α-Ti matrix, as shown in Figs. 19*a, b*. As shown in Fig. 19*c*, the compressive stress–strain curves highlight its excellent mechanical properties, including compressive yield strength up to 1593 MPa, compressive strength of over 2400 MPa, and fracture strain to 26.8% due to this particular microstructure. The significant strengthening in the present Ti–Cu alloys can be rationalized by second-phase strengthening and fine-grained strengthening.

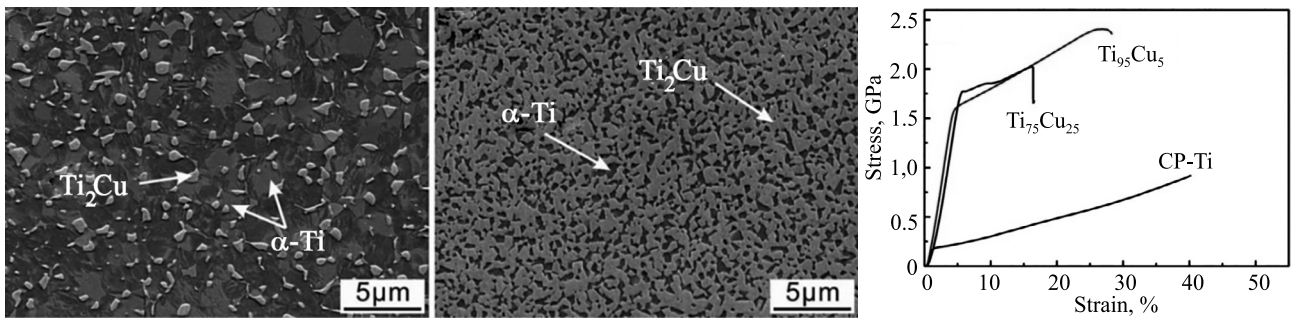

a *b* *c*

Fig. 19. SEM images of the microstructure of spark plasma sintered $Ti_{95}Cu_5$ (*a*) and $Ti_{75}Cu_{25}$ (*b*) alloys; compressive stress–strain curves (*c*) of spark plasma sintered $Ti_{95}Cu_5$ and $Ti_{75}Cu_{25}$ alloys [104]

Carbon nanotubes (CNTs) were usually used as a proper reinforcement to generate aluminum matrix composites via advanced SPS technology to improve the strength and corrosion properties of the Al alloy. In 2014, my group used a low sintering temperature (673~823 K), high holding pressure (300 MPa), and short holding time (6 min) to restrain grain growth, avoid agglomeration, and accelerate the densification process of the bulk nanocrystalline aluminum [105]. The result indicated that NC-aluminum sintered at 773 K possessed a small grain size of 80 nm, high tensile strength of 282 MPa, an outstanding compressive strength of 665 MPa, as well as a super micro-hardness of 3.06 GPa.

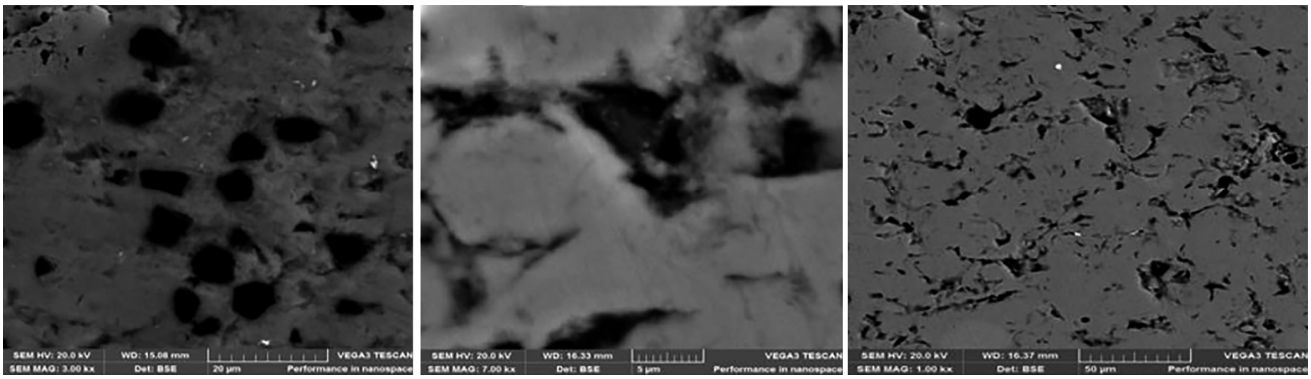

a *b* *c*

Fig. 20. The SEM of sintered samples: pure Al (*a*), Al–1CNTs (*b*), and Al–4CNTs (*c*) [106]

Figure 20 shows the microstructure of sintered pure Al, Al–1CNTs, and Al–4CNTs composite. It can be seen that grain growth and voids were not observed in the microstructure. Furthermore, CNTs were homogeneously dispersed in the Al matrix. The results showed that Al–4CNTs exhibited the highest microhardness of 482.60 ± ± 12 MPa, representing 27% improvement in monolithic Al alloy due to grain refinement, high densification, and cohesive grain boundaries [106].

MAGNESIUM AND MAGNESIUM ALLOY

Magnesium and magnesium alloys have been paid extensive attention for potential applications in automotive, aerospace, microelectronics, and bio industries due to the performance advantages, including low density, high damping capacity, and high specific strength. Microstructural optimization using powder metallurgy technology has been proposed to overcome the low mechanical property of Mg alloys used as lightweight engineering materials. As a typical powder metallurgy technique, spark plasma sintering has become the most widely-used densification method for powders due to its high heating efficiency, low sintering temperature, and short sintering time. In particular, the advantage of limiting the grain growth during the sintering process allows producing fine-grained metals and composites. Hence, the SPS technique has been increasingly adopted to improve the characteristic of the Mg alloys.

Muhammad et al. [107] reported that a high sintering temperature of 552–585°C (0.84–0.88T_m, were T_m is melting point) was required to obtain nearly fully dense Mg and AZ31 alloy by SPS. In Lee et al.' work [108], fine-grained Mg–6 wt.% Al alloy with high toughness and corrosion resistance is fabricated by using degassing process before SPS and proper sintering parameters. It is concluded that a thinner and discontinuous oxide distribution at PBs formed due to higher degassing vacuum levels, resulting in solid interfaces by facilitating the easy breakup of the oxide film. Properly sintering at 530°C with adequate degassing allows complete connection across PBs as well as a fine grain micro-structure shown in Table 1 and Fig. 21. In Liu's study [109], a high-strength aluminum-magnesium interface structure (maximum interfacial bonding strength reached 59.96 MPa) was prepared by spark plasma sintering. Microstructural observations indicate that phase transformations from solid to liquid layers

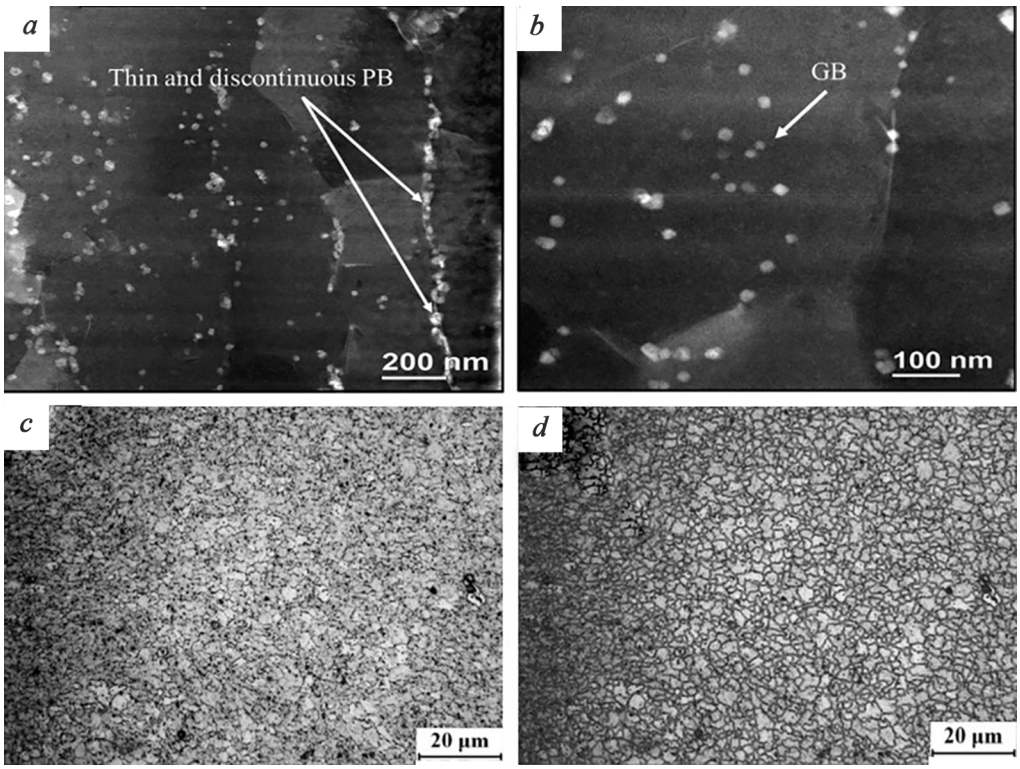

Fig. 21. TEM micrographs of PBs with different degassing conditions sintered at 530°C for 20 min: *a*) incomplete degassing ($2 \cdot 10^{-3}$ torr at 450°C for 60 min); *b*) appropriate degassing ($2 \cdot 10^{-7}$ torr at 450°C for 60 min); *c*) optical micrographs; *d*) I-solution image showing grain size of the Mg–6 wt.% Al alloys sintered at 530°C with appropriate degassing for the SPS process [108]

TABLE 1. Average Grain Size Measured Using an I-Solution DT Program

Sample	Average grain size, μm	Sample	Average grain size, μm
510°C ($2 \cdot 10^{-3}$ Torr)	3.54	530°C ($2 \cdot 10^{-7}$ Torr)	3.63
510°C ($2 \cdot 10^{-7}$ Torr)	3.56	560°C ($2 \cdot 10^{-7}$ Torr)	10.41

occurred with an increase in sintering pressure, affecting local temperature and materials diffusion. The growth of cracks can be subsequently hindered because of the fine-grain structure in the liquid layer, resulting in the increased interface performance.

OTHER METAL ALLOYS

Copper and Copper Alloys. Zhang (Beijing Institute of Technology) [5] consolidated nano-sized copper powder using the SPS method and investigated the relationship between the sintering temperature and relative density, microstructure, and the mechanical properties of the nanocrystalline bulk copper. As shown in Fig. 22, the microstructure evolution and the sintering temperature changes during the SPS illustrate the sintering neck's appearance, growth, and connection, as shown in Figs. 22*a–d*. As shown in Fig. 22*e*, the nanocrystalline copper's yield strength and the relative density first increased and then decreased with the increasing SPS temperature. Finally, the yield strength (nearly 650 MPa) and relative density (greater than 99%) were obtained under the optimal SPS parameters. In another work [110], the influence of SPS temperature on the microstructure and mechanical properties of the in-situ synthesized discontinuous three-dimensional graphene-like network (3DGN)

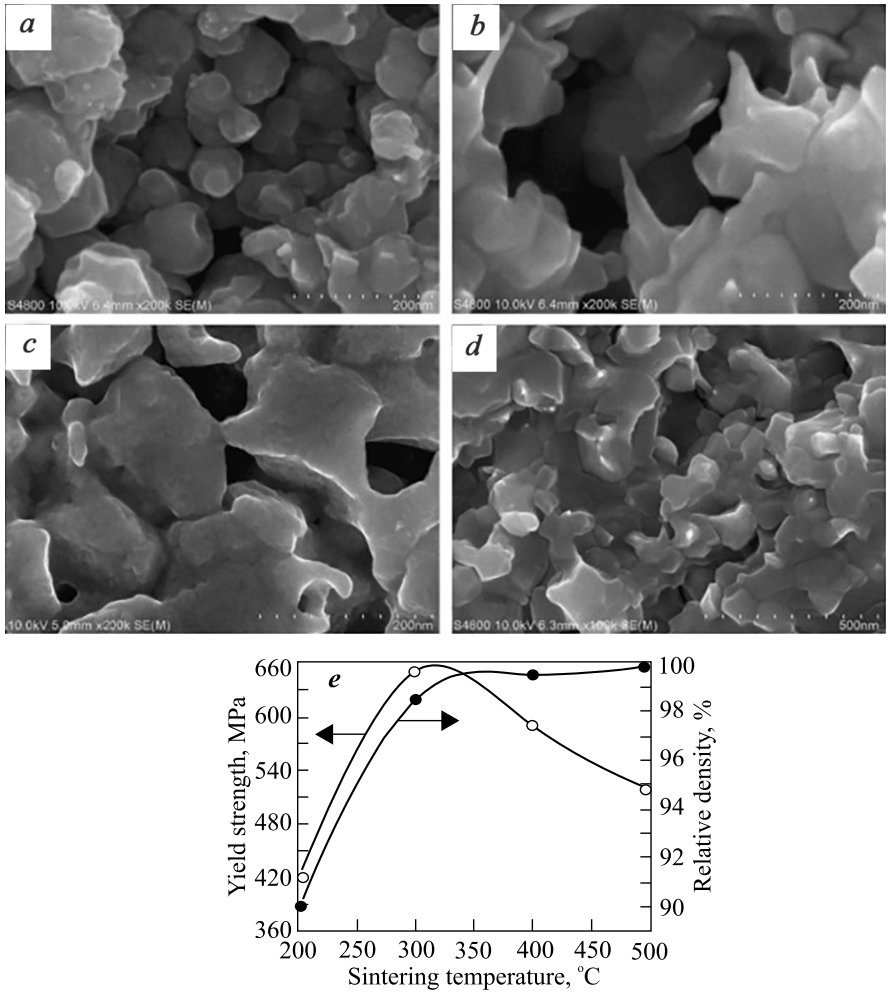

Fig. 22. Typical microstructures, relative density, and yield strength as a function of the NC bulk copper temperature: *a*) emergence of the sintering neck; *b*) growth of the sintering neck; *c*) connection of the sintering neck; *d*) microstructure after rapid densification; *e*) curves of a versus [5]

reinforced copper matrix composites were investigated. It demonstrates that with the rise of the sintering temperature from 600 to 700°C, the GN distribution changes from intergranular to intragranular type due to the significant improvement in interfacial wettability.

Furthermore, the overall mechanical performance of the GN/Cu composites presents an unanticipated declining trend at elevated sintering temperatures due to the combined effects of grain growth, defect increment, and interfaces at elevated temperatures. For the Cu and Cu alloys, the SPS temperature is an essential factor for microstructure and properties. Selecting appropriate sintering temperature is beneficial to acquire corresponding structure and performance.

High Entropy Alloys. The high entropy alloys (HEA) as a new class of alloys, also called multi-component alloys, have been attracting much attention in various fields worldwide due to their unique properties since they were first introduced in 2004 [111, 112]. Each of the significant elements in HEA has a concentration between 5 and 35 at.% with high mixing entropy in their liquid state. The concentration can be tailored to enhance many promising properties, such as high hardness, wear resistance, excellent high and low-temperature strength, and good resistance to oxidation and corrosion. The most widely used approach to fabricating HEA bulk materials is vacuum arc melting, yielding HEA materials with complete density. However, there is a significant drawback of causing micro-segregation and large-elongated columnar grain structure formation during solidification. Using the advanced spark plasma sintering technology, considered as a candidate synthetic route, the HEAs with near-full-density and

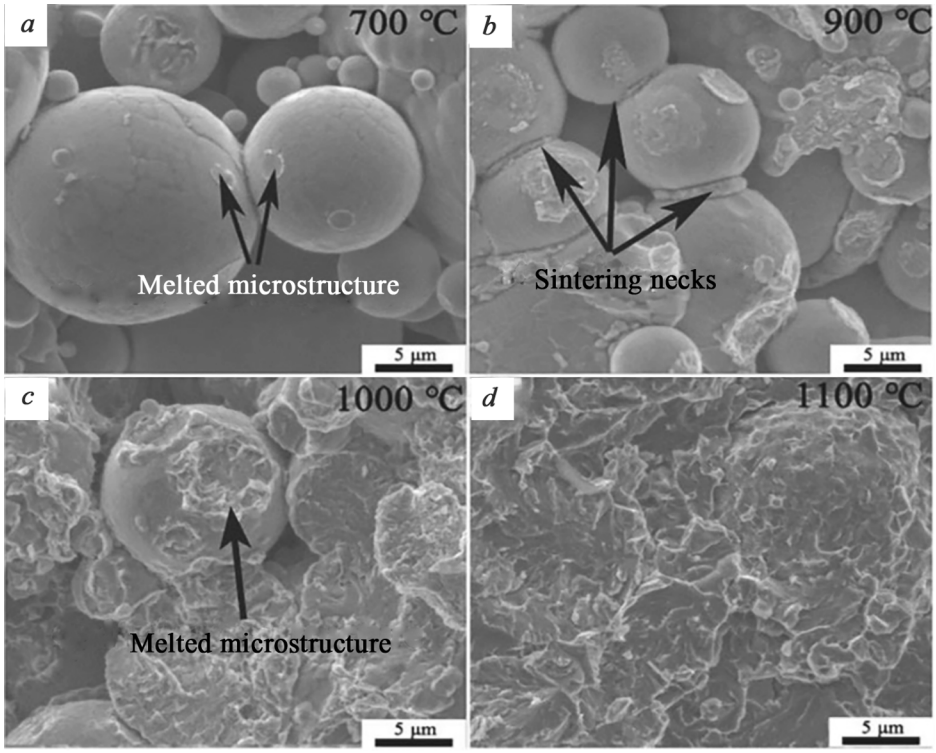

Fig. 23. The sintering characteristics of pre-powders at different temperatures [113]

uniform microstructure can be produced due to the guarantees of short alloying time, efficient cooling, the operation in a controlled atmosphere, and the low energy consumption [52, 113].

Zhou [113] fabricated the AlCoCrFeNi alloy with a good combination of strength and compression limit (~2368 MPa, 22.1%) through various gas atomization and spark plasma sintering at 1100°C. The sintering characteristics of the powders at a few representative temperatures presented in Fig. 23 demonstrate that with the increasing of sintering temperature, the sintered parts were more and more consolidated to total density. This microstructure evolution during the sintering was mainly attributed to the ease of atomic diffusion between powders, excitation of plasma which would lean to local melting, and the deformation of powder. The equiatomic CoCrNiCuZn HEA powder was successfully consolidated by mechanical alloying and SPS [114]. The results show that Vickers hardness and compressive strength of the consolidated alloy sintered at 900°C were 615 HV and 2121 MPa, respectively, indicating excellent mechanical properties.

Zhiqiang Fu [60] successfully fabricated bulk $Fe_{25}Ni_{25}Co_{25}Ti_{15}Al_{10}$ HEA characterized by the high tensile strength of 2.52 GPa, a minor bcc phase (~17.7 vol.%), together with a primary fcc phase (~82.3 vol.%) via mechanical alloying followed by SPS consolidation. The results prove that phase formation mechanisms have a significant effect on the mechanical performance of HEAs. Besides, the secondary γ* precipitates within the γ' precipitates were formed because of the nonequilibrium SPS process. The above successful examples indicate that temperature, atomic diffusion, and phase transformation are highly important for microstructural evolution and the final performance of the HEA. Therefore, the SPS could be used as an alternative fabrication for HEAs due to the easy control of these influence factors.

CONCLUDING REMARKS AND OUTLOOK

As a novel sintering method, SPS has exhibited many significant advantages in fabricating advanced metal structure materials compared to other conventional sintering methods. Its unique function in accelerating densification of powder/bulk products and controlling surface atom-diffusion, grain size, and phase transformation greatly enhanced the free degree of material design. Various novel metal materials with high performance, including high-quality special steels, novel lightweight alloy materials, high entropy alloys, and other metal alloys,

have been successfully developed using SPS. Spark plasma sintering can be used not only for rapidly and efficiently consolidating powder-based materials but also for welding different/same parts together and realizing high-through preparation of materials. Besides developing PSPS, high pressure, and current SPS, the SPE and FSPS devices have provided achievable access to the design and fabricate large-size dense-bulks with unique microstructures.

Based on the above representation, the most noteworthy feature of the SPS densification mechanism lies in the generation of spark discharge and high-temperature plasma associated with pulsed DC, which plays a significant role in improving surface condition, promoting atom diffusion, and decreasing the flow stress of the materials. The indirect thermal effect associated with DC pulse current resulting in heat generation and Joule heating contributes significantly to the rapid densification of the materials during the SPS process. Additionally, it can be concluded that most sintering parameters have a double effect of positive and negative in sintering behavior. So, suitable sintering processes and parameters must be selected and set to obtain bulk materials with specific textures and excellent properties.

Though the SPS technique has been used in various materials in recent decades successfully, its outstanding advantages are caused by the simultaneous existence of pressing, thermal, electromagnetic fields and their complicated coupling effects in the SPS process. However, the interaction mechanisms between particles are debatable. Therefore, microstructural and physical phenomena during the SPS and their effects on material densification still require deep examination. Moreover, the developments of mold design for preparing various materials with large size, complicated shape, and unique microstructure are becoming more and more critical.

Additionally, it is another noteworthy research direction on conducting an experimental study to examine the actual temperature in the SPS samples. There is no doubt that the more advanced and multifunctional SPS devices will emerge soon to continuously improve the service level of materials.

ACKNOWLEDGEMENTS

The National Science Foundation of China supported this work (Grant No. 51374039), the Chinese Defense Advance Research Program of Science and Technology (Grant No. 41422010905), and the National Defense Foundation of China (Grant No. 6142902010603). The authors acknowledge Dr. Zhengyang Hu and Dr. Weiguo Wang for their help with discussions and suggestions during the preparation of this manuscript.

REFERENCES

1. M. Omori, “Sintering, consolidation, reaction and crystal growth by the spark plasma system (SPS),” *Mater. Sci. Eng. A*, **287**, 183–188 (2000).
2. V. Nečina and W. Pabst, “Influence of the heating rate on grain size of alumina ceramics prepared via spark plasma sintering (SPS),” *J. Eur. Ceram. Soc.*, **40**, 3656–3662 (2020).
3. D. Paraskevas, S. Dadbakhsh, J. Vleugels, K. Vanmeensel, W. Dewul, and J.R. Duflou, “Solid state recycling of pure Mg and AZ31 Mg machining chips via spark plasma sintering,” *Mater. Des.*, **109**, 520–529 (2016).
4. R.F Liu., W.X. Wang, H.S. Chen, M.B. Tan, and Y.Y. Zhang, “Microstructure evolution and mechanical properties of micro-/nano-bimodal size B_4C particles reinforced aluminum matrix composites prepared by SPS followed by HER,” *Vacuum*, **151**, 39–50 (2018).
5. Z.H. Zhang, F.C. Wang, S.K. Lee, Y. Liu, J.W. Cheng, and Y. Liang, “Microstructure characteristic, mechanical properties and sintering mechanism of nanocrystalline copper obtained by SPS process,” *Mater. Sci. Eng. A*, **523**, 134–138 (2009).
6. V.N. Chuvildeev, D.V. Panov, M.S. Boldin, A.V. Nokhrin, Yu.V. Blagoveshchensky, N.V. Sakharov, S.V. Shotin, and D.N. Kotkov, “Structure and properties of advanced materials obtained by spark plasma sintering,” *Acta Astronaut.*, **109**, 172–176 (2015).
7. V.N. Chuvildeev, A.V. Nokhrin, and V.I. Kopylov, “Spark plasma sintering for high-speed diffusion bonding of the ultrafine-grained near-αTi–5Al–2V alloy with high strength and corrosion resistance for nuclear engineering,” *J. Mater. Sci.*, **54**, 14926–14949 (2019).

8. E.A. Olevsky, S. Kandukuri, and L. Froyen, "Consolidation enhancement in spark-plasma sintering: Impact of high heating rates," *J. Appl. Phys.*, **102**, 114913 (2007).
9. S.R. Oke, O.O. Ige, O.E. Falodun, B.A. Obadele, M.B. Shongwe, and P.A. Olubambi, "Optimization of process parameters for spark plasma sintering of nano structured SAF 2205 composite," *J. Mater. Res. Technol.*, **7**, 126–134 (2017).
10. Z.H. Zhang, Z.F. Liu, J.F. Lu, X.B. Shen, F.C. Wang, "The sintering mechanism in spark plasma sintering-proof of the occurrence of spark discharge," *Scr. Mater.*, **81**, 56–59 (2014).
11. J.H. Liu, Z.Y. Fu, W.M. Wang, J.Y. Zhang, H. Wang, Y.C. Wang, S. Lee, and K. Niihara, "Ultra-high heating rate densification of nanocrystalline magnesia at high pressure and investigation on densification mechanisms," *J. Eur. Ceram. Soc.*, **34**, 3095–3102 (2014).
12. J.Y. Zhang, F.C. Meng, R.I. Todd, and Z.Y. Fu, "The nature of grain boundaries in alumina fabricated by fast sintering," *Scr. Mater.*, **62**, 658–661 (2010).
13. D.K. Guan, W.M. Rainforth, J. Sharp, J.H. Gao, and I. Todd, "On the use of cryomilling and spark plasma sintering to achieve high strength in a magnesium alloy," *J. Alloys Compd.*, **688**, 1141–1150 (2016).
14. S.H. Deng, H.J. Zhao, R.D. Li, T.C. Yuan, L.B. Li, and P. Cao, "The influence of the local effect of electric current on densification of tungsten powder during spark plasma sintering," *Powder Technol.*, **356**, 769–777 (2019).
15. G. Lee, C. Maniere, J. McKittrick, R. Doerner, D. Nishijima, A. Gattuso, T. Abrams, D. Thomas, C. Back, and E.A. Olevsky, "Consolidation of Molybdenum nanopowders by spark plasma sintering: Densification mechanism and first mirror application," *J. Nucl. Mater.*, **516**, 354–359 (2019).
16. C.L. Cramer, J.W. McMurray, M.J. Lance, and R.A. Lowden, "Reaction-bond composite synthesis of SiC–TiB_2 by spark plasma sintering/field-assisted sintering technology (SPS/FAST)," *J. Eur. Ceram. Soc.*, **40**, 988–995 (2020).
17. Z.H. Zhang, X.B. Shen, C. Zhang, S. Wei, S.K. Lee, and F.C. Wang, "A new rapid route to in-situ synthesize TiB–Ti system functionally graded materials using spark plasma sintering method," *Mater. Sci. Eng*. A, **565**, 326–332 (2013).
18. Z.H. Zhang, X.B. Shen, F.C. Wang, and S.K. Lee, "A New Rapid Route for In Situ Synthesizing Monolithic TiB Ceramic," *J. Am. Ceram. Soc.*, **94**, 2754–2756 (2011).
19. S. Sovizi and M.E. Seraji, "The Densification Behavior of Metals and Alloys During Spark Plasma Sintering: A Mini-Review," *Sci. Sintering*, **51**, 135–152 (2019).
20. A.I. Raichenko, G.L. Burenkov, A.F. Khrienko, and V.P. Litvinenko, "Electric discharge sintering of binary powder mixtures," *Powder Metall. Met. Ceram.*, **15**, 602–606 (1976).
21. O. Ertorer, T. Topping, Y. Li, W. Moss, and E. Lavernia, "Nanostructured Ti consolidated via spark plasma sintering," *Metall. Mater. Trans. A*, **42**, 964–973 (2011).
22. D. Demirskyi and O. Vasylkiv, "Consolidation and grain growth of tantalum diboride during spark plasma sintering," *Ceram. Int.*, **42**, 16396–16400 (2016).
23. R.Z. Valiev, R.K. Islamgaliev, N.F. Kuzmina, Y. Li, and T.G. Langdon, "Strengthening and grain refinement in an Al-6061 metal matrix composite through intense plastic straining," *Scr. Mater.*, **40**, 117–122 (1998).
24. Z.H. Zhang, F.C. Wang, L. Wang, and S.K. Li, "Ultrafine-grained copper prepared by spark plasma sintering process," *Mater. Sci. Eng. A*, **476**, 201–205 (2008).
25. R. Sule, P.A. Olubambi, I. Sigalas, J.K.O. Asante, and J.C. Garrett, "Effect of SPS consolidation parameters on submicron Cu and Cu-CNT composites for thermal management," *Powder Technol.*, **258**, 198–205 (2014).
26. Z.Y. Hu, Z.H. Zhang, X.W. Cheng, F.C. Wang, Y.F. Zhang, and S.L. Li, "A review of multi-physical fields induced phenomena and effects in spark plasma sintering: Fundamentals and applications," *Mater. Des.*, **191**, 108662 (2020).
27. A.G. Bloxam, *GB Patent, No. 9020* (1906).

28. G.F. Taylor, *US Patent No.1, 896, 854* (1933).
29. I. Sulima, P. Putyra, P. Hyjek, and T. Tokarski, "Effect of SPS parameters on densification and properties of steel matrix composites," *Adv. Powder Technol.*, **26**, 1152–1161 (2015).
30. E.G. Grigoriev and AV. Rosliakov, "Electro-discharge compaction of WC-Co and W-Ni-Fe-Co composite materials," *J. Mater. Process. Technol.*, **191**, 182–184 (2007).
31. A. Leich, Röttger, W. Theisen, and M. Krengel, "Densification of nanocrystalline NdFeB magnets processed by electro-discharge sintering-Microstructure, magnetic, and mechanical properties," *J. Magn. Magn. Mater.*, **460**, 454–460 (2018).
32. F. Balima, F. Bellin, D. Michau, O. Viraphong, A. Poulon-Quintin, U.C. Chung, A. Dourfaye, and A. Largeteau, "High pressure pulsed electric current activated equipment (HP-SPS) for material processing," *Mater. Des.*, **139**, 541–548 (2018).
33. F. Balima and A. Largeteau, "Phase transformation of alumina induced by high pressure spark plasma sintering (HP-SPS)," *Scr. Mater.*, **158**, 20–23 (2019).
34. R. Yamanoglu, "A perspective from conventional sintering to accelerated sintering without pressure," *Powder Metall. Met. Ceram.*, **57**, 513–525 (2019).
35. M.N. Ge, X.F. Wang, G.Y. Li, C. Lu, J.F. Zhang, and R. Tu, "Synthesis of Cr_2AlC from elemental powders with modified pressureless spark plasma sintering," *J. Wuhan Univ. Technol., Mater. Sci. Ed.*, **34**, 287–292 (2019).
36. W.L. Bradbury and E.A. Olevsky, "Production of SiC-C composites by free-pressureless spark plasma sintering (FPSPS)," *Scr. Mater.*, **63**, 77–80 (2010).
37. Y.S. Lin, M.A. Meyers, and E.A. Olevsky, "Microchannelled hydroxyapatite components by sequential freeze drying and free pressureless spark plasma sintering," *Adv. Appl. Ceram.*, **111**, 269–274 (2012).
38. L. Bertolla, I. Dlouhý, P. Tatarko, A. Viani, A. Mahajan, Z. Chlup, M.J. Reece, and A.R. Boccaccini, "Pressureless spark plasma-sintered Bioglass®; 45S5 with enhanced mechanical properties and stress-induced new phase formation," *J. Eur. Ceram. Soc.*, **37**, 2727–2736 (2017).
39. D.V. Dudina, B.B. Bokhonov, and A.K. Mukherjee, "Formation of aluminum particles with shell morphology during pressureless spark plasma sintering of Fe–Al mixtures: Current-related or Kirkendall effect," *Materials*, **9**, 375 (2016).
40. R. Yamanoglu, N. Gulsoy, E.A. Olevsky, and H.O. Gulsoy, "Production of porous $Ti_5Al_{2.5}Fe$ alloy via pressureless spark plasma sintering," *J. Alloys Compd.*, **680**, 654–658 (2016).
41. R. Hallett, J.R. Cox, and K. Morsi, "Novel Spark Plasma Extrusion of Titanium Above and Below the β-Transus: Effect on Microstructure and Properties," *Metall. Mater. Trans. B*, **51**, 1363–1369 (2020).
42. K. Morsi, A.M.K. Esawi, P. Borah, S. Lanka, A. Sayed, and M. Taher, "Properties of single and dual matrix aluminum-carbon nanotube composites processed via spark plasma extrusion (SPE)," *Mater. Sci. Eng. A*, **527**, 5686–5690 (2010).
43. J.H. Yang, J. Trapp, Q.G. Guo, and B. Kieback, "Joining of 316L stainless steel by using spark plasma sintering method," *Mater. Des.*, **52**, 179–189 (2013).
44. K. Park, D. Kim, K. Kim, and H. Kwon, "Aluminum/Stainless Steel Clad Materials Fabricated via Spark Plasma Sintering," *Materials*, **13**, 239 (2020).
45. Z.Y. Fu, W. Ji, and W.M. Wang, "Recent Progress in Flash Sintering Technology of Ceramic Materials," *J. Chin. Ceram. Soc.*, **45**, 1211–1219 (2017).
46. F. Gucci, T.G. Saunders, B. Srinivasan, F. Cheviré, D.A. Ferluccio, J.W.G. Bos, and M.J. Reece, "Hybrid Flash-SPS of $TiNiCu_{0.05}Sn$ with reduced thermal conductivity," *J. Alloys Compd.*, **837**, 155058 (2020).
47. C. Manière, U. Kus, G. Chevallier, A. Weibel, L. Durand, J. Huez, D. Delagnes, and C. Estournèss, "How to overcome the main challenges of SPS technology: Reproducibility, multi-samples and elaboration of complex shapes," *Spark Plasma Sintering*, 77–108 (2019).
48. O.E. Falodun, B.A. Obadele, S.R. Oke, A.M. Okoro, and P.A. Olubambi, "Titanium-based matrix composites reinforced with particulate, microstructure, and mechanical properties using spark plasma sintering technique: a review," *Int. J. Adv. Des. Manuf. Technol.*, **102**, 1689–1701 (2019).

49. S.R. Oke, O.O. Ige, O.E. Falodun, A.M. Okoro, M. R. Mphahlele, and P.A. Olubambi, "Powder metallurgy of stainless steels and composites: a review of mechanical alloying and spark plasma sintering," *Int. J. Adv. Des. Manuf. Technol.*, **102,** 3271–3290 (2019).
50. E. Jajarmi, L. Desogus, R. Orrùa, S.A. Sajjadi, and G. Cao, "On the fabrication of functional graded 3Y-PSZ/316L materials by SPS: Process optimization and characterization of the obtained products," *Ceram. Int.*, **42**, 8351–8359 (2016).
51. Z.A. Munir, D.V. Quach, and M. Ohyanagi, "Electric current activation of sintering: A review of the pulsed electric current sintering process," *J. Am. Ceram. Soc.*, **94**, 1–19 (2011).
52. O. Guillon, J. Gonzalez-Julian, B. Dargatz, T. Kessel, G. Schierning, J. Räthel, and M. Herrmana, "Field-assisted sintering technology/spark plasma sintering: mechanisms, materials, and technology developments,".*Adv. Eng. Mater.*, **16**, 830-849 (2014).
53. Z.Q. Fu, W.P. Chen, H.M. Wen, Z. Chen, and E.J. Lavernia, "Effects of Co and sintering method on microstructure and mechanical behavior of a high-entropy $Al_{0.6}NiFeCrCo$ alloy prepared by powder metallurgy," *J. Alloys Compd.*, **646**, 175–182 (2015).
54. S.X. Song, Z. Wang, and G.P. Shi, "Heating mechanism of spark plasma sintering," *Ceram. Int.*, **39**, 1393–1396 (2013).
55. N. Chawake, L.D. Pinto, A.K. Srivastav, K. Akkiraju, B.S. Murty, and R.S. Kottada, "On Joule heating during spark plasma sintering of metal powders," *Scr. Mater.*, **93**, 52–55 (2014).
56. K. Vanmeensel, A. Laptev, J. Hennicke, J. Vleugels, and O.V.D. Biest, "Modelling of the temperature distribution during field assisted sintering," *Acta Mater.*, **53**, 4379–4388 (2005).
57. S. Ghosh, A.H. Chokshi, P. Lee, and R. Raj, "A huge effect of weak dc electrical fields on grain growth in zirconia," *J. Am. Ceram. Soc.*, **92**, 1856–1859 (2009).
58. C. Romaric, L. Sophie, N. Foad, C. Frederic, B. Guillaume, F. Gilbert, C. Jean-Marc, and B. Frederic, "Effect of current on the sintering of pre-oxidized copper powders by SPS," *J. Alloys Compd.*, **692**, 478–484 (2017).
59. A. Bachmaier, M. Pfaff, M. Stolpe, H. Aboulfadl, and C. Motz, "Phase separation of a supersaturated nanocrystalline Cu-Co alloy and its influence on thermal stability," *Acta Mater.*, **96**, 269–283 (2015).
60. R. Marder, C. Estournès, G. Chevallier, and R. Chaim, "Plasma in spark plasma sintering of ceramic particle compacts," *Scr. Mater.*, **82**, 57–60 (2014).
61. M. Tokita, "Development of large-size ceramic/mrtal bulk FGM fabricated by spark plasma sintering," *Mater. Sci. Forum*, **308–311**, 83–88 (1999).
62. Z.Q. Fu, A. Hoffman, B.E. MacDonald, Z.F. Jiang, W.P. Chen, M. Arivu, H.M. Wen, and E.J. Laverni, "Atom probe tomography study of an $Fe_{25}Ni_{25}Co_{25}Ti_{15}Al_{10}$ high-entropy alloy fabricated by powder metallurgy," *Acta Mater.*, **179**, 372–382 (2019).
63. T. Nagae, M. Yokota, M. Nose, S. Tomida, T. Kamiya, and S. Saji, "Effects of pulse current on an aluminum powder oxide layer during pulse current pressure sintering," *Mater. Trans.*, **43**, 1390–1397 (2005).
64. M. Omori, T. Hirai, Material and composite formation by spark plasma system (SPS), in: M. Miyake and M. Samandi, *Proceedings of the First Symposium on Microwave, Plasma and Thermo-Chemical Processing of Advanced Materials*, Osaka University (1997).
65. R.D.Li, T.C. Yuan, X.J. Liu, J.W. Wang, H. Wu, F.H. Zeng, and X.Z. Hou, "Microstructural evolution and sintering kinetics during spark plasma sintering of Fe and Al blended powder," *Trans. Nonferrous Met. Soc. China*, **27**, Issue 7, 1594–1601 (2017).
66. W.A. Salandro, J.J. Jones, C. Bunget, L. Mears, and J.T. Roth, "The effect of electric current on metals," *Springer International Publishing,* 37–54 (2015).
67. J. Narayan, "A new mechanism for field-assisted processing and flash sintering of materials," *Scr. Mater.*, **69**, 107–111 (2013).
68. C.M. Tan and A. Roy, "Electromigration in ULSI interconnects," *Mater. Sci. Eng, R*, **58**, 3-75 (2007).

69. K. Hu, Q.X. Li, S.G. Qu, and Y.Y. Li, "Spark-Plasma Sintering of W-5.6Ni-1.4Fe Heavy Alloys: Densification and Grain Growth," *Mater. Trans. A*, **44**, 923-933 (2013).
70. D. Empl, L. Felberbaum, V. Laporte, D. Chatain, and A. Mortensen, " Dihedral angles in Cu-1wt.% Pb: Grain boundary energy and grain boundary triple line effects," *Acta Mater.*, **57**, 2527-2537 (2009).
71. S.Y. Xie, R.D. Li, T.C. Yuana, M. Zhang, M.B. Wang, L. Yin, and P. Cao, "Effect of phase transformation on densification kinetics and properties of spark plasma sintered $Al_{0.7}$CoCrFeNi high-entropy alloy," *Mater. Charact.*, **160**, 11009 (2020).
72. C.B. Danisman, B. Yavas, O. Yucel, F. Sahin, and G. Goller, "Processing and characterization of spark plasma sintered TZM alloy," *J. Alloys Compd*, **685**, 860–868 (2016).
73. D.M. Liu, Y.H. Xiong, T. Troy, Y.Z. Zhou, C. Haines, J. Paras, D. Martin, D. Kapoor, J. Schoenung, and E. Lavernia, "Spark plasma sintering of cryomilled nanocrystalline Al alloy-Part II: influence of processing conditions on densification and properties," *Metall. Mater. Trans. A*, **43**, 340–350 (2012).
74. A. Chua, M. Brochu, and D. Bishop, "Spark plasma sintering of prealloyed aluminium powders," *Powder Metall.*, **58**, 51-60 (2015).
75. C.K. Kim, S. Lee, S.Y. Shin, and D.H. Kim, "Effects of consolidation temperature and pressure on microstructures and mechanical properties of Cu-based bulk amorphous alloys consolidated by spark plasma sintering," *J. Alloys Compd.*, **453**, 108-114 (2008).
76. M. Zadra, F. Casari, L. Girardini, A. Molinari, "Microstructure and mechanical properties of cp-titanium produced by spark plasma sintering," *Powder Metall.*, **51**, 59-65 (2008).
77. I.U.H. Toor, J. Ahmed, M.A. Hussein, and N. Al-Aqeeli, "Optimization of process parameters for spark plasma sintering of nano-structured ferritic Fe–18Cr–2Si alloy," *Powder Technol*., **299**, 62–70 (2016).
78. M.I. Makena, M.B. Shongwe, M.M. Ramakokovhu, and P.A. Olubambi, "Effect of sintering parameters on densification, corrosion and wear behaviour of Ni–50Fe alloy prepared by spark plasma sintering," *J. Alloys Compd.*, **699**, 1166–1179 (2017).
79. G.A. Sweet, M. Brochu, R.L. Hexemer Jr, I.W. Donaldson, and D.P. Bishop, "Microstructure and mechanical properties of air atomized aluminum powder consolidated via spark plasma sintering," *Mater. Sci. Eng. A*, **608**, 273–282 (2014).
80. T.H. De Keijser, J.I. Langford, E.J. Mittemeijer, and A.B.P. Vogels, "Use of the Voigt function in a single-line method for the analysis of X-ray diffraction line broadening," *J. Appl. Crystall.*, **15**, 308–314 (1982).
81. G. Marnier, C. Keller, J. Noudem, and E. Hug, "Functional properties of a spark plasma sintered ultrafine-grained 316L steel," *Mater. Des.*, **63**, 633–640 (2014).
82. D. Garbiec and P. Siwak, "Study on microstructure and mechanical properties of spark plasma sintered Alumix 431 powder," *Powder Metall.*, **59**, 242–248 (2016).
83. A.H. Barry, G. Dirras, F. Schoenstein, F. Tétard, and N. Jouini, "Noureddine Jouini, Microstructure and mechanical properties of bulk highly faulted fcc/hcp nanostructured cobalt microstructures," *Mater. Charact.*, **91**, 26–33 (2014).
84. M. Pellizzari, A. Fedrizzi, and M. Zadra. "Influence of processing parameters and particle size on the properties of hot work and high speed tool steels by spark plasma sintering," *Mater. Des.*, **32**, 1796–1805 (2011).
85. O. Ertorer, T. Topping, Y. Li, W. Moss, and E. Lavernia, "Nanostructured Ti consolidated via spark plasma sintering," *Mater. Trans. A*, **42**, 964–973 (2011).
86. M.B. Shongwe, M.M. Ramakokovhu, S. Diouf, M.O. Durowoju, B.A. Obadele, R. Sule, M.L. Lethabane, and P.A. Olubambi, "Effect of starting powder particle size and heating rate on spark plasma sintering of FeNi alloys," *J. Alloys Compd.*, **678**, 241–248 (2016).
87. K. Hu, X.Q. Li, C. Yang, and Y.Y. Li, "Densification and microstructure evolution during SPS consolidation process in W–Ni–Fe system," *Trans. Nonferrous Met. Soc. China*, **21**, 493–501 (2011).
88. R. Yamanoglu, W. Bradbury, E. Karakulak, E.A. Olevsky, and R.M. German, "Characterisation of nickel alloy powders processed by spark plasma sintering," *Powder Metall.*, **57**, 380–386 (2014).

89. P. Unifantowicz, Z. Oksiuta, P. Olier, Y. de Carlan, and N. Baluc, "Microstructure and mechanical properties of an ODS RAF steel fabricated by hot extrusion or hot isostatic pressing," *Fusion Eng. Des.*, **86**, 2413–2416 (2011).
90. D. Pazos, M. Suárez, A. Fernández, P. Fernández, I. Iturriza, and N. Ordás, "Microstructural comparison of Oxide Dispersion Strengthened Fe-14Cr steels produced by HIP and SPS," *Fusion Eng. Des.*, **146**, 2328–2333 (2019).
91. A. García-Junceda, E. Macía, D. Garbiec, M. Serrano, J. M. Torralba, and M. Campos, "Effect of Small Variations in Zr Content on the Microstructure and Properties of Ferritic ODS Steels Consolidated by SPS,"*Metals*, **10**, 348 (2020).
92. M. Pellizzari, A. Fedrizzi, and M. Zadra, "Spark plasma Co-sintering of mechanically milled tool steel and high speed steel powders," *Materials*, **9**, 482 (2016).
93. A. Farid, A. Liaqat, P.Z. Feng, and A.S. Jawad, "Enhanced sintering, microstructure evolution and mechanical properties of 316L stainless steel with $MoSi_2$ addition," *J. Alloys Compd.*, **509**, 8794–8797 (2011).
94. N. Kurgan, "Effects of sintering atmosphere on microstructure and mechanical property of sintered powder metallurgy 316L stainless steel," *Mater. Des.*, **52**, 995–998 (2013).
95. H. Fallahdoost, H. Khorsand, R. Eslami-Farsani, and E. Ganjeh, "On the tribological behavior of nanoalumina reinforced low alloy sintered steel," *Mater. Des.*, **57**, 60–66 (2014).
96. D. Chaira, "Development of nano-structured duplex and ferritic stainless steels by pulverisette planetary milling followed by pressureless sintering," *Mater. Charact.*, **99**, 220–229 (2015).
97. A. Almathami and M. Brochu, "Microstructure and transformation of Al-containing nanostructured 316L stainless steel coatings processed using spark plasma sintering," *J. Mater. Process. Technol.*, **210**, 2119–2124 (2010),
98. Z.H. Hu, K.J. Ning, and K. Lu, "Study of spark plasma sintered nanostructured ferritic steel alloy with silicon carbide addition," *Mater. Sci. Eng. A*, **670**, 75-80 (2016).
99. S.R. Oke, O.O. Ige, O.E. Falodun, M.R. Mphahlele, and P.A. Olubambi, "Densification behavior of spark plasma sintered duplex stainless steel reinforced with TiN nanoparticles," *IOP Conf. Ser.: Mater. Sci. Eng.*, **430**, 012034 (2018).
100. A. Mohammadzadeh, A.S. Namini, M. Azadbeh, and A. Motallebzadeh, "On the physical and mechanical properties of spark plasma sintered pure Ti and Ti–TiB composite," *Mater. Res. Express*, **5**, 126512 (2018).
101. Z.G. Li, A.P. Dong, H. Xing, H. Xu, D.F. Du, T. Zhang, H. She, D.H. Wang, G.L. Zhu, and B.D. Sun, "Microstructure and mechanical properties of bimodal Ti–Bi alloys fabricated by mechanical alloying and spark plasma sintering for biomedical applications," *Mater. Charact.*, **161**, 110134 (2020).
102. O.J. Akinribide, G.N. Mekgwe, B.A. Obadele, O.O. Ajibola, S.O. Akinwamide, and P.A. Olubambi, "Microstructural and phase evolution of spark plasma sintering of graphitized $Ti(C_{0.9}N_{0.1})$ composites," *Int. J. Refract. Met. Hard Mater.*, **78**, 164–169 (2019).
103. B.A. Obadele, O.E. Falodun, S.R. Oke, and P.A. Olubambi. "Spark plasma sintering behaviour of commercially pure titanium micro-alloyed with Ta–Ru," *Particul. Sci. Technol.*, **37**, 890–896 (2019).
104. R. Dong, W.W. Zhu, C.C. Zhao, Y.W. Zhang, and F.Z. Ren, "Microstructure, Mechanical Properties, and Sliding Wear Behavior of Spark Plasma Sintered Ti–Cu Alloys," *Metall. Mater. Trans. A*, **49**, 6147 (2018).
105. Z.F. Liu, Z.H. Zhang, J.F. Lu, A.V. Korznikov, E. Korznikova, and F.C. Wang, "Effect of sintering temperature on microstructures and mechanical properties of spark plasma sintered nanocrystalline aluminum," *Mater. Des.*, **64**, 625–630 (2014).
106. C.O. Ujah, A.P.I. Popoola, O.M. Popoola, V.S. Aigbodion, "Influence of CNTs addition on the mechanical, microstructural, and corrosion properties of Al alloy using spark plasma sintering technique," *Int. J. Adv. Des. Manuf. Technol.*, **106**, 2961–2969 (2020).
107. W.N.A.W. Muhammad, Z. Sajuri, Y. Mutoh, Y. Miyashita, "Microstructure and mechanical properties of magnesium composites prepared by spark plasma sintering technology," *J. Alloy. Comp.*, **509**, 6021–6029 (2011).

108. C.S. Lee, H.C. Lee, G.H. Kimb, J.H. Hanc, and W.J. Kimd, "Design of Mg–6 wt.% Al alloy with high toughness and corrosion resistance prepared by mechanical alloying and spark plasma sintering," *Mater. Charact*, **158**, 109995 (2019).
109. Y. Liu, Y.Z. Ma, W.S. Liu, Y.F. Huang, L. Wu, T. Wang, C. Liu, and L. Yang, "The mechanical properties and formation mechanism of Al/Mg composite interface prepared by spark plasma sintering under different sintering pressures," *Vacuum*, **176**, 109300 (2020).
110. C. Sun, X. Zhang, N.Q. Zhao, and C.N. He, "Influence of spark plasma sintering temperature on the microstructure and strengthening mechanisms of discontinuous three-dimensional graphene-like network reinforced Cu matrix composites," *Mater. Sci. Eng. A*, **756**, 82–91 (2019).
111. J.W. Yeh, S.K. Chen, S.J. Lin, J.Y. Gan, T.S. Chin, T.T. Sun, C.H. Tsau, and S.Y. Chang, "Nanostructured high-entropy alloys with multiple principal elements: novel alloy design concepts and outcomes," *Adv. Eng. Mater.*, **6**, 299–303 (2004).
112. L. Liu, L.J. He, J.G. Qi, B. Wang, Z.F. Zhao, J. Shang, and Y. Zhang, "Effects of Sn element on microstructure and properties of $Sn_xAl_{2.5}FeCoNiCu$ multi-component alloys," *J. Alloy Compd.*, **654**, 327–332 (2016).
113. P.F. Zhou, D.H. Xiao, Z. Wu, and M. Song, "Microstructure and mechanical properties of AlCoCrFeNi high entropy alloys produced by spark plasma sintering," *Mater. Res. Express*, **6**, 0865e7 (2019).
114. Y.C. Sun, B. Ke, Y.L. Li, K. Yang, M.Q. Yang, W. Ji, and Z.Y. Fu, "Phases, microstructures and mechanical properties of CoCrNiCuZn high-entropy alloy prepared by mechanical alloying and spark plasma sintering," *Entropy*, **21**, 122 (2019).